Semiannual Technical Report

Growth and Doping of $Al_xGa_{1-x}N$ Films by Electron Cyclotron Resonance Assisted Molecular Beam Epitaxy

ONR Grant No. N00014-92-J-1436
(May 1, 1992 - April 30, 1993)

P.I. Theodore D. Moustakas

Department of Electrical,
Computer, and Systems Engineering

Boston Univeristy
Boston, MA 02215
617-353-5431

Approved for Public Release; Distribution Unlimited

October 30, 1992

REPORT DOCUMENTATION PAGE

Form Approved
OMB No 0704-0188

1. AGENCY USE ONLY (Leave blank)	2. REPORT DATE	3. REPORT TYPE AND DATES COVERED
	30 Oct. 1992	Semiannual 01 May 1992 - 30 Apr 1993

4. TITLE AND SUBTITLE
Growth and Doping of Al_xGa_{1-x} Films by Electron Cyclotron Resonance Assisted Molecular Beam Epitaxy

5. FUNDING NUMBERS
R&T: 4145329---01
S.O: 1114SS
AGO: N66017
CAGE: 3A817

6. AUTHOR(S)
Moustakas, Theodore D.

7. PERFORMING ORGANIZATION NAME(S) AND ADDRESS(ES)
Boston University
College of Engineering
44 Cummington St.
Boston, MA 02215

8. PERFORMING ORGANIZATION REPORT NUMBER
N00014-92-J-1436

9. SPONSORING/MONITORING AGENCY NAME(S) AND ADDRESS(ES)
Department of the Navy
Office of the Chief of Naval Research
800 North Quincy St, Code 1511:KIJ
Arlington, VA 22217-5000

10. SPONSORING/MONITORING AGENCY REPORT NUMBER

11. SUPPLEMENTARY NOTES

12a. DISTRIBUTION/AVAILABILITY STATEMENT
Approved for Public Release; Distribution Unlimited

12b. DISTRIBUTION CODE
N00179

13. ABSTRACT (Maximum 200 words)

Growth and doping of GaN by ECR assisted MBE is reported. We report on the role of the GaN-buffer and AlN-buffer, and their combination on the two dimensional nucleation rate and lateral growth rate. Conditions for quasi layer by layer growth were identified. XRD was used to study secondary phase, the [illegible] direction and quality of orientational ordering in and out of the substrate, and homogeneous and inhomogeneous strain. Relatively high mobility autodoped films were produced and their transport mechanism was investigated. Intrinsic GaN-films were produced and were doped n- and p-type with Si and Mg respectively, without requiring annealing for dopant activation. RIE processing of GaN was developed and metal contacts were investigated. A direct correlation between the metal work function and barrier height was also found.

14. SUBJECT TERMS
Gallium Nitride, Aluminum Gallium Nitride, Molecular Beam Epitaxy, Electron Cyclotron Resonance source, n-doping, p-doping, Ohmic contacts

15. NUMBER OF PAGES
89

16. PRICE CODE

17. SECURITY CLASSIFICATION OF REPORT	18. SECURITY CLASSIFICATION OF THIS PAGE	19. SECURITY CLASSIFICATION OF ABSTRACT	20. LIMITATION OF ABSTRACT
UNCLAS	UNCLAS	UNCLAS	

Table of Contents

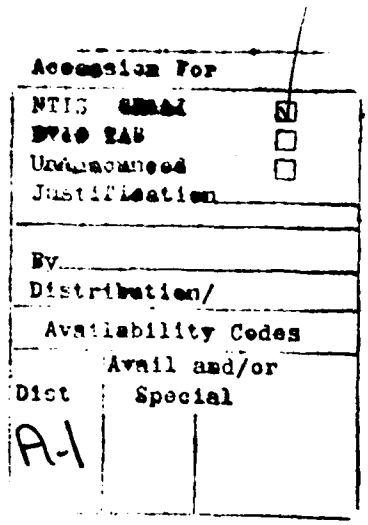

1 Summary of results during the first six months of the current funding period

During the first funding year the work is focused on the heteropitaxial growth and doping of GaN films by the method of Electron Cyclotron Resonance microwave plasma assisted Molecular Beam Epitaxy. A brief description of specific accomplishements during the first six months of the current grant are listed below:

1.1 Heteroepitaxial growth of GaN by ECR-assisted MBE.

The heteroepitaxial growth of GaN on a variety of substrates [Si(100), Si(111), sapphire (c, α, R-planes)] by the ECR-MBE method was investigated, using a two step growth process for GaN which specifically separates the nucleation and growth phases. Since the nucleation rate depends exponentially on $1/T$ it is clear that the nucleation dominated regime occurs at low temperatures. Thus, we developed a low temperature buffer which covers uniformly the substrate due to the large nucleation rate. The growth of the rest of the film occurs at relatively higher temperatures and should be close to homoepitaxy. Under equilibrium conditions, homoepitaxy should proceed in the layer-by-layer mode without the formation of nuclei. However, due to imperfections of the buffer layer, nuclei may form at the suface edges and steps at small contact angles. Recently we were able to form GaN film with an extermely low two-dimensional nucleation rate ($\sim$ 20nuclei/μm^2 · h) and lateral growth rate 100 times the vertical growth rate. Thus, under these conditions, the growth is quasi *layer-by-layer*. (1,2)

Besides the GaN-buffer, we have recently developed an AlN buffer not by a deposition process but by nitridation of the sapphire substrate. We found that the conversion of Al_2O_3 surface to AlN requires exposing the substrate, held at 850°, to an ECR nitrogen plasma for approximately 10-15 min. This AlN layer appears to be atomically smooth based on the elongated RHEED pattern(2,3). We found that the GaN-buffer, which is usually grown at lower temperatures (approximately 400° C), is atomically smooth, when grown on the top of this AlN buffer. Furthermore, GaN films grown on the combination of AlN-GaN buffers were found to have the best surface morphology with lateral growth rate much higher than the vertical growth rate. Details of these results are presented in Appendix A.

1.2 Atomic Structure Studies.

The structure of GaN films grown on a variety of substrates [Si(100), Si(111), sapphire (c, α, R-planes)] was studied with four-circle X-ray diffractometry. These studies allowed us to determine the presence of secondary phases, the direction and quality of orientational ordering in and out of the substrate plane and the homogeneous and inhomogeneous strains in the film. Our studies show that wurtzite and zincblende GaN polymorphs often coexist in films which grow with their close-packed stacking planes parallel to the substrate. The evidence suggests that the zincblende phase may nucleate at stacking faults (4). Details on these studies are described in Appendix B.

1.3 Growth of High mobility GaN films and transport mechanism in GaN.

We have been able to grow auto-doped GaN films systematically with carrier concentrations from 10^{19} to 2×10^{17}cm^{-3}. Simultaneously, the electron mobility increased from about 20 cm^2/V-sec to 210 cm^2/V-sec. These results are illustrated in Fig. 1. It is interesting to note that this curve extrapolates to a mobility of 600 cm^2/V-sec reported for GaN films grown by the MOCVD method (5). Based on the temperature dependent transport measurements, a picture of simultaneous transport in the conduction band and the autodoping centers has emerged. When the concentration of the autodoping centers becomes less than the concentration of the deep defects, the material becomes fully compensated, leading to hopping conduction in the deep compensating defects, accounting for the low electron mobility in these films(6). Details on these studies are presented in Appendix C.

1.4 n- and p-doping of GaN films.

Plasma modes with high nitrogen plasma density were identified which allow the growth of semi-insulating GaN films.

Such GaN films were doped n-type with Si, a common dopant in MBE growth. Silicon was incorporated as a donor with a net carrier concentration of $N_D - N_A = 2 \times 10^{18}$cm^{-3}.

GaN films produced under the growth conditions which lead to intrinsic films were doped p-type by the incorporation of Mg. Carrier concentrations up to 2×10^{19} were obtained without requiring an additional annealing step as reported previously (5,7). These studies are still in progress and will continue during the second half of the funding year.

1.5 Ohmic Contacts / Processing of GaN.

Reactive Ion Etching (RIE) techniques have been developed to process GaN films. Etching was carried out in Freon 12, at 140Å/min and selectivity 3:1 for GaN/photoresist (8).

The rectification properties of various metal contacts to GaN were investigated. A direct correlation between the metal work functions and barrier height to GaN was found, a result attributed to the ionic character of GaN. Thus, ohmic contacts to both n- and p-type GaN can be made by choosing metals with the appropriate work functions (Al for n-type and Au for p-type) (9). Details on these studies can be found in Appendix D.

Figure 1.

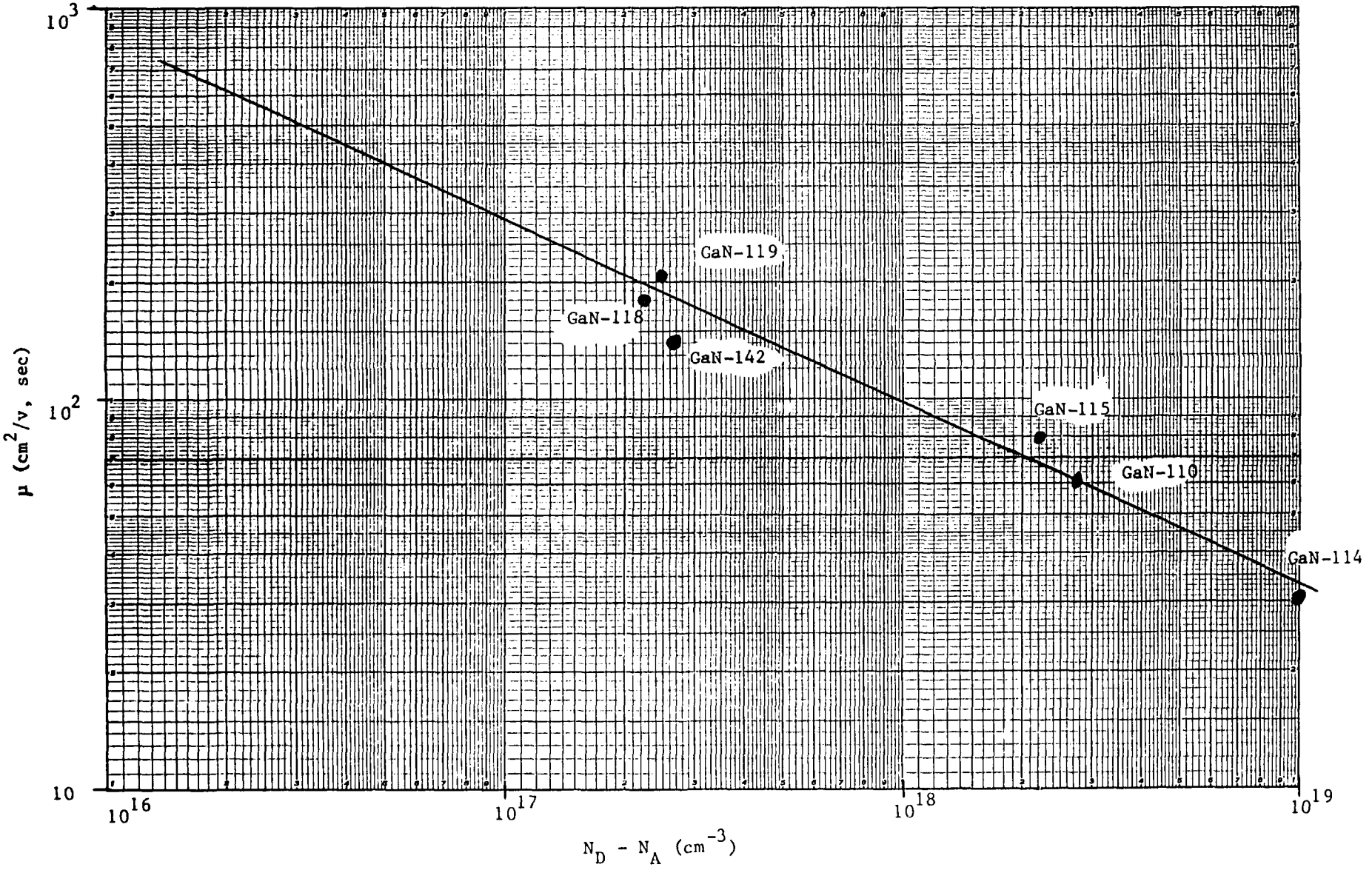

References:

1. "Epitaxial growth and characterization of zinc-blende gallium nitride on (001) silicon," T. Lei, T.D. Moustakas, R.J. Graham, Y. He, and S.J. Berkowitz, J. Appl. Phys. 71, 4933 (1992).

2. "Growth of GaN by ECR-Assisted MBE," T.D. Moustakas, T. Lei, and R.J. Molnar, Physica B: Condensed Matter (Accepted for Publication).

3. "A Comparative Study of GaN Films Grown on Different Faces of Sapphire by ECR-Assisted MBE," T.D. Moustakas, R.J. Molnar, T. Lei, G. Menon, and C.R. Eddy Jr., Mat. Res. Soc. Symp. Proc. Vol. 242, 427 (1992).

4. "Heteroepitaxy, Polymorphism, and Faulting in GaN Thin Films on Silicon and Sapphire Substrates," T. Lei, K.F. Ludwig Jr, and T.D. Moustakas, J. Appl. Phys. (Submitted for Publication).

5. "Conductivity Control of AlGaN, Fabrication of AlGaN/GaN Multiheterostructures and Their Application to UV/Blue Light Emitting Devices," I. Akasaki and H. Amano, Mat. Res. Soc. Symp. Proc. Vol. 242, 383 (1992).

6. "Electron Transport Mechanism in Gallium Nitride," R.J. Molnar, T. Lei, and T.D. Moustakas, Appl. Phys. Lett. (Jan. 1993).

7. "Thermal Annealing Effects on P-Type Mg-Doped GaN films," S. Nakamura, T. Mukai, M. Senoh, and N. Iwasa, Jpn. J. Appl. Phys. Vol. 31, L139 (1992).

8. "Ohmic Contacts and Schottky Barriers on Gallium Nitride," J. Foresi, M.S. Thesis (Boston University, 1992).

9. "Metal Contacts to Gallium Nitride," J. Foresi and T.D. Moustakas, Appl. Phys. Lett. (submitted for publication).

Appendix A:

Growth of GaN by ECR-Assisted MBE

accepted for publication:
Physica B: Condensed Matter

Growth of GaN by ECR-Assisted MBE

T. D. Moustakas, T. Lei, and R. J. Molnar
Molecular Beam Epitaxy Laboratory
Department of Electrical, Computer and Systems Engineering
Boston University, Boston, MA 02215

Abstract

High quality GaN films have been grown on a variety of substrates by Electron Cyclotron Resonance microwave plasma-assisted Molecular Beam Epitaxy (ECR-MBE). The films were grown in two steps. First, a GaN-buffer was grown at low temperature and then the rest of the film was grown at higher temperatures. We found that this method of growth leads to a relatively small two-dimensional nucleation rate ($\sim$ 20 nuclei/$\mu m^2 \cdot h$) and high lateral growth rate (100 times faster than the vertical growth rate). This type of quasi-layer-by-layer growth results in smooth surface morphology to within 100Å. Growth on Si(100) leads to single crystalline GaN films having the zinc-blende structure. Growth on Si(111) leads to GaN films having the wurtzitic structure with large concentration of stacking faults. The crystallographic orientation and the surface morphology of GaN films on sapphire depends on the orientation of sapphire. To this date, the best films were grown on the basal plane of sapphire.

1 Introduction

The family of refractory nitrides (InN, GaN, and AlN), their solid solutions and heterojunctions are one of the most promising families of electronic materials. All three are direct bandgap semiconductors with their energy gaps covering the region from 1.95eV (InN)and 3.4eV (GaN) to 6.28eV (AlN). Thus, the growth of high quality crystals and successful doping of these materials should lead to applications in optoelectronic devices from the visible to the ultraviolet part of the electromagnetic spectrum, as well as in devices for high power and high temperature electronics [1-2]. GaN, in particular, was predicted to have a high electron drift velocity, so it should also be suitable for high frequency and microwave devices [3].

GaN films have been grown by many growth techniques, including Chemical Vapor Deposition [4-7], Metal-Organic Chemical Vapor Deposition [8-15], Molecular Beam

Epitaxy [16-25], and a number of plasma-assisted processes [26-30]. A variety of substrates such as silicon, spinel, silicon carbide, and various crystallographic orientations of sapphire have been used in these studies. Most of the films grown are wurtzitic (α-GaN), and have n-type conductivity with high carrier concentration [31], which is believed to result from nitrogen vacancies [31-32] or oxygen impurity incorporation [33]. P-type conductivity has been reported recently on Mg-doped GaN films [34-35].

Zincblende GaN(β-GaN), which is the thermodynamically metastable phase of GaN, is hoped to be more amenable to doping than the wurtzitic GaN, since all of the III-V compounds that can be efficiently doped n-type or p-type are cubic [2]. β-GaN has been epitaxially stabilized on β-SiC and MgO(100) substrate [18-19], which are closely lattice-matched to β-GaN, and on GaAs [36-37] and Si substrate [21-25] which have significant mismatch to β-GaN.

In this paper, we review the growth of GaN films by the Electron Cyclotron Resonance microwave plasma-assisted Molecular Beam Epitaxy. Particular emphasis is placed on the growth of this material in two temperature steps which was developed recently in our laboratory [21-25,38]. Films were grown on Si(100), Si(111), and various faces of sapphire.

2 Experimental Methods

The deposition system used in this study is schematically illustrated in Fig. 1. Two ECR sources were used. The first (Astex 8" model 1000) was used for the growth of GaN on Si(100) and Si(111). The second (Astex compact model) was used for the growth of GaN on sapphire. The pressure in the overall system was 10^{-11} Torr. A Reflection High Energy Electron Diffraction (RHEED) setup is an integral part of the apparatus. A conventional Knudsen effusion cell was used to evaporate gallium. Atomic and ionic nitrogen were produceed by passing molecular nitrogen through the ECR source. Part of the molecular nitrogen was also introduced downstream of the ECR source. Typically, 10% of the molecular nitrogen gas is converted into atomic nitrogen. Due to this high decomposition rate, a source pressure of about 10^{-4} Torr is sufficient for the growth of stoichiometric films. The magnetic field configuration for the 8" source under optimized conditions for the growth of GaN films is illustrated in Fig. 2. The on-axis ECR condition (H = 835 Gauss) is about 40 cm above the substrate. The compact ECR source fits inside an effusion cell and thus the distance from the front of the source to the substrate is only 12 cm.

The structure and microstructure of the films were studied by Reflection High Energy Electron Diffraction (RHEED), X-ray diffraction and Scanning Electron Microscopy (SEM). X-ray diffraction studies were performed using a diffractometer with

four-circle geometry. This allows us to perform ϕ-scans at a reflection peak (hkl), corresponding to planes not parallel to the substrate to probe in-plane ordering. Additionally, standard θ-2θ scans were performed to probe the ordering normal to the substrate.

Si(001) and Si(111) substrates (n-type, p-type or undoped) were used in these studies. They were ultrasonically degreased in solvents and etched in buffered HF to remove the oxides, prior to their introduction into the MBE unit. In the preparation chamber, the substrates were outgassed for 15 minutes at 850°C.

The sapphire substrates were subjected to the following cleaning steps prior to the growth of the GaN films. They were sequentially cleaned in ultrasonic baths of trichloroethylene, acetone, and isopropanol for removal of hydrocarbon residues from the surface, etched in H_3PO_4 : H_2SO_4 (1:3) for the removal of surface contaminants and mechanical damage due to polishing and finally rinsed in de-ionized water. After these steps, the substrates were blown dry with nitrogen, mounted on a molybdenum block and transferred to the introduction chamber of the MBE system. In the preparation chamber, the substrates were heated to 850°C for approximately half an hour and then transferred to the growth chamber where they were subjected to bombardment by nitrogen plasma for approximately half an hour at 700°C.

3 Experimental Results

3.1 Growth on Si(100)

Following cleaning, the Si substrate was examined by studying its RHEED pattern in the growth chamber at 400°C. Fig. 3 shows typical RHEED patterns of the Si substrate with the electron beam incident along [100] and [110] directions. These results clearly indicate that the Si(001) surface is unreconstructed (i.e. 1 x 1). We find that such an unreconstructed Si(001) surface is required to epitaxially grow a single crystalline GaN-buffer. Outgassing of the Si substrate at lower temperatures, for example 600°C, leads to an irregular pattern with few diffraction spots, which we were unable to index with any reconstruction pattern. A GaN-buffer grown on such a surface would generally be polycrystalline with the wurtzitic structure. It is conceivable that epitaxy of GaN should take place on a well ordered unreconstruted surface, but not on an irregular disordered surface.

After the substrate preparation and characterization, a GaN-buffer layer of about 300Å to 900Å thich was deposited at a temperature of 400°C for 10 to 30 minutes, Fig. 4 shows the RHEED patterns at two azimuthal incidence of the electron beam for the GaN buffer layer. The diffraction spots are relatively broad, signifying that

the thin buffer layer is very defective. This is expected due to the large lattice mismatch between the film and the substrate. However, the symmetry of the patterns indicates that the buffer layer has the zincblende structure with the [001] direction perpendicular to the substrate.

Following the deposition and characterization of the GaN-buffer the substrate was heated to a higher temperature, typically 600°C, and a GaN film of about 1 μm thick was grown at a growth rate about 2000Å/h. Shown in Fig. 5 (a) and (b) are typical RHEED patterns of a GaN film about 1 μm thick grown on a p-type substrate for [100] and [110] azimuthal incidence of the electron beam. The results are similar when the growth takes place on undoped substrates. These results clearly indicate that the GaN film has the zincblende structure, with its (001) crystallographic planes parallel to the substate surface. The diffraction spots of this pattern are significantly sharper and elongated, which suggests that the final GaN film has a better crystalline quality and a smoother surface morphology than the GaN-buffer.

The RHEED pattern of a GaN film grown on a p-type substrate under slightly lower nitrogen pressure is shown in Fig. 6. The streak-like pattern is characteristic of two dimensional scattering, indicating that the GaN film is close to atomically smooth. Such elongated RHEED patterns were frequently observed when the growth took place on n-type substrates. This may suggest that GaN wets to the n-type substrate better than the p-type substrate. Morimoto and co-workers reported that in vapor phase growth, GaN adhered to n-type silicon, but not to p-type silicon substrates.

In a few cases, the Si substrate was first bombarded with nitrogen plasma prior to the formation of the GaN buffer. The lack of a RHEED pattern indicates that either an amorphous SiN film was formed on the substrate or that the surface was disordered. The GaN buffer grown on nitrogen plasma bombarded substrates were found to be polycrystalline having the wurtzitic structure with the (0002) preferred orientation.

Shown in Fig. 7 are the surface morphology and the cross-sectional view of a β-GaN film on a p-type silicon substrate studied by SEM. It can be seen that the film has a relatively flat surface, roughened with many well-oriented rectangular shaped 'tiles', which reflect the symmetry of the β-GaN (001) surface. The cross-sectional view shows no evidence of columnar morphology, which is another indication that the film is single crystalline.

Detailed electron microscopy studies [23] have shown that the tiles in Fig. 7 are oriented along the [110] and [1$\bar{1}$0] directions. This presumably arises because the GaN surfaces corresponding to those directions are more closely packed than the [100] and [010] surfaces and therefore have lower surface energy.

Shown in Fig. 8 (a) is the morphology of the GaN film, whose RHEED pattern was discussed in Fig. 6. The surface morphology of a film on an n-type substrate is shown in Fig. 8 (b). Both of these surfaces are smooth with steps approximately $100\mathring{A}$ thick, which resulted from a layer-by-layer growth [23]. These results suggest that additional optizimation of the growth process could lead to atomically smooth surfaces.

From the data of Fig. 8, we can calculate the two-dimensional nucleation rate and the lateral growth rate. Let J be the nucleation rate, s be the average area of the plateau, h be the height of the plateau, and t be the time for the plateau to grow, which is limited by nucleation. Then, we have

$$\sqrt{s} \simeq v_l t = \frac{v_l}{(Js)} \tag{1}$$

and

$$h \simeq v_n t = \frac{v_n}{(Js)} \tag{2}$$

where v_l and v_n are the lateral and vertical growth rates respectively. From the data of Fig. 8, we have $\sqrt{s} \simeq 1\mu$m and $h \simeq 100\mathring{A}$. If we use the known vertical growth rate $v_n = 2000\ \mathring{A}$/h, then from (1) and (2) we obtain $v_l \simeq 100 V_n$ and J $\simeq$ 20 nuclei/(μm^2·h).

These data indicate that this two-step method of film growth leads to quasi-layer-by-layer growth with very small two-dimensional nucleation rate and high lateral growth rate.

The structure of the films was confirmed by Convergent Beam Electron Diffraction (CBED) and Selected Area Diffraction (SAD). These studies were published elsewhere [23]. In this paper, we focus on the X-ray diffraction studies of the films.

The X-ray diffraction in Fig. 9 shows a strong peak at $2\theta = 40.1$ degrees, whose d-spacing is 2.25 $\mathring{A}$, which is due to (002) reflection from β-GaN. Hence, the lattice constant to β-GaN was found to be 4.50 $\mathring{A}$, in good agreement with the electron diffraction data [23]. A small peak was also observed at $2\theta = 34.6$, which is due to the d-spacing of (111) β-GaN or (0002) α-GaN. This suggests that the GaN film has some misoriented domains. These domains may have developed in the early stages of the buffer layer deposition as revealed by TEM imaging [39]. Similar structural faults have also been observed in the interface between GaN epitaxy on GaAs(100) [37]. We have also observed these misoriented domains in almost all of our samples. The consistent appearance of the misoriented domains in GaN-Si and GaN-GaAs heteroepitaxy is very likely to be related to the large lattice mismatch between the GaN and the substrate. Because of the large lattice mismatch, the interface of GaN and the substrate is under significant strain; therefore, it might be favorable for the system

to introduce dislocations or misorientations of GaN to reduce the interfacial energies. In zincblende or wurtzitic structures, the [111] or [0002] planes are the most closely packed, and hence have the lowest surface energies. Therefore, the introduction of [111] or [0002] oriented GaN would lower the surface energy at the GaN-vapor interface, and would not necessarily increase the energy for the GaN-substrate interface, since it was strained significantly. However, the [111] or [0002] oriented GaN domains would grow slower than the [001] oriented GaN grains stabilized by introduction of dislocations. As a result, they were buried in the interface region as the film grew.

The X-ray rocking curve of the [002] peak of a GaN film 4 μm thick was found to have a Full Width at Half Maximum (FWHM) of approximately 60 minutes, which measures the orientation spread perpendicular to the substrate. This is significantly narrower than that of GaN on GaAs [37], but much broader than that of β-GaN on MgO substrates [19] and α-GaN on [0001] sapphire substrates as discussed later.

The ϕ-scan for the zincblende GaN was performed at the [$\bar{1}$11] reflection, and is shown in Fig. 10. The data clearly show that the peak repeats itself every 90 degrees, consistent with the cubic symmetry of this material. The FWHM of these peaks, which measures the in-plane orientation spread, was found to be 2.5 degrees.

3.2 Growth on Si(111)

Growth on Si(111) followed the same steps as described previously in the growth on Si(001). Fig. 11 shows the RHEED pattern for a GaN film on Si(111). The data indicate that the film has the wurtzitic structure with the [0001] planes parallel to the substrate. The sharpness of the diffraction spots indicate good crystalline quality of the film.

Fig. 12 shows a θ-2θ scan for a GaN film on Si(111). The single peak at 34.6 degrees corresponds to [0002] reflection of the wurtzitic GaN; thus, the lattice constant in the c-direction is 5.18 $\AA$

The ϕ-scan for the wurtzitic GaN shown in Fig. 13 was performed at the [1$\bar{1}$02] reflection. Clearly, this peak repeats every 60 degrees, consistent with the 3 mm symmetry of the rotation axis. The FWHM is found to be 1.9 degrees, while the FWHM of the θ-2θ rocking curve at the [0002] peak is found to be 0.9 degrees.

The XRD data of Fig. 12 and Fig. 13 appear to indicate that the α-GaN film on Si(111) is a single crystal. However, any stacking faults along the growth direction of the GaN film on Si(111) can not be easily detected in the normal θ-2θ scans [40]. Such stacking faults are very common defects in materials with the FCC or HCP structures growing along the [111] and [0002] directions [40]. Such stacking faults, if they exist in the wurtzitic GaN films on Si(111), should give rise to a certain amount of cubic GaN component with the [111] planes parallel to the substrate. To explore this possibility,

we rotated the sample in such a way that the X-ray diffraction corresponds to the [002] reflection of the zincblende structure, and indeed a peak was detected at $2\theta = 40$ degrees. This is shown in a θ-2θ scan around this peak (see Fig. 14).

To obtain a stronger reflection, ϕ-scans on these cubic domains were performed at $[\bar{1}11]$ peak, which is shown in Fig. 15. These data reveal a repetition every 60 degrees. Since the [111] axis in the zincblende structure is only a 3-fold rotational axis, the ϕ-scan should show a repetition every 120 degrees instead of every 60 degrees. Therefore differing by 60 degrees in ϕ. This can be accounted for if there are two kinds of stacking sequences, namely ABC... and CBA... sequence. The fact the peak at $\phi = 60$ degrees is of comparable intensity to the other two peaks suggests that the two types of stacking sequences occur with an equal probability, as is expected.

The existence of the cubic GaN domains in the wurtzite structures implies the existence of high concentration of stacking faults. This could be due to the fact that the cohesive energies of wurtzite and zincblende GaN are comparable, so that the formation energy of a stacking fault is negligible. If this is true, then all of the [0002] oriented GaN films have a considerable amount of stacking faults. This is currently being investigated by XRD studies of GaN on $[11\bar{2}0]$ and [0001] sapphire substrates. However, one should not rule out that the high concentration of stacking faults in GaN on Si(111) is related to strain resulting from the large lattice mismatch between GaN and Si, which could lead to reduction of the formation energy of stacking faults due to structural deformation.

3.3 Growth on Sapphire Substrate

GaN films were also grown on the c-plane [0001], a-plane $[11\bar{2}0]$ and r-plane $[1\bar{1}02]$ of sapphire. Fig. 16 shows RHEED patterns of the three types of substrates after the exposure to the nitrogen plasma. The data indicate that the surface of the substrates were nitrided and from the diffraction patterns, the lattice constant of the AlN was estimated to be a = 3.1 $\AA$. Furthermore, the streakiness of the diffraction patterns, in particular those of the c-plane and a-plane sapphire substrates, suggests that the AlN layers are atomically smooth.

Fig. 17 shows RHEED patterns of the GaN-buffer on the three types of substrates. The data indicate that the GaN-buffer is single crystalline on all three types of substrates. The GaN films grown on the c-plane and a-plane sapphire substrates have their c-plane [0001] parallel to the substrates, while the GaN films grown on the r-plane of sapphire have their a-plane $[11\bar{2}0]$ parallel to the substrate. The streakiness of the diffraction patterns of the GaN-buffers on the c-plane and a-plane sapphire substrates suggests that the GaN-buffer on these substrates are atomically smooth.

Fig. 18 shows RHEED patterns of the GaN films at the end of each run. These

reveal the same epitaxial relationship between GaN films and the substrates as the corresponding GaN-buffers discussed in Fig. 17. Also, the films on the c-plane and a-plane sapphire substrates are atomically smooth.

Fig. 19 shows the surface morphology of GaN films grown on the three types of substrates. The films on the a-plane have the smoothest surface morphology. The surface morphology of GaN films on the c-plane consists of interconnected tiles several thousand angstroms in size. The GaN films grown on the r-plane sapphire were found to have the roughest surface morphology. The pyramidal surface morphology is likely to be related to the fact that the a-plane of GaN is bounded by two prism planes under equilibrium growth conditions.

Fig. 20 shows the θ-2θ XRD and the θ-rocking curve at the main reflection peak of the GaN films grown on the three types of substrates. The main reflection peak for the GaN films grown on the c-plane and a-plane sapphire occurs at $2\theta = 34.6$ degrees, corresponding to the [0002] reflection. This confirms that films were grown with their c-planes parallel to the substrate. The main diffraction peak of the GaN film on the r-plane of sapphire occurs at $2\theta = 57.8$ degrees corresponding to the GaN $[11\bar{2}0]$ reflection. This confirm the RHEED study that the a-plane of the GaN film is parallel to the substrate. The rocking curve of the GaN film on the c-plane of sapphire has the smallest width (FWHM = 10 min.), indicating that the crystalline quality of these films to be the best. Such films were also found to have the highest electron mobility ($\mu > 200$ cm^2/V·s) among films grown by MBE processes.

The epitaxial relationship of the GaN films to the c-plane of sapphire is to be expected. However, the epitaxial relationship of the GaN films on the a-plane and r-plane of sapphire is not obvious. This epitaxial relationship can be accounted for as follows: The a-plane sapphire has a rectangular unit cell with dimensions 12.97 $\AA$ x 8.23 $\AA$, two of which can accomodate a number of unit cells of GaN basal planes as illustratedin Fig. 21 (a). This results in 1.6% lattice mismatch along [0001] of sapphire and 0.6% along $[1\bar{1}00]$ axis of the sapphire substrate. The r-plane of sapphire substrate has a unit cell with dimensions 4.75 $\AA$ x 15.34 $\AA$, which accomodates three unit cells of the a-plane of GaN as illustrated in Fig. 21 (b). This results in 16% lattice mismatch along the $[11\bar{2}0]$ of sapphire and 1.3% along the $[1\bar{1}01]$ of sapphire.

4 Conclusion

In conclusion, a two step growth process has been developed for the heteroepitaxial growth of GaN films. This method was found to lead to films with smooth surface morphology, which we interpreted as resulting from a quasi-layer-by-layer growth. Using this process GaN films were grown on a variety of substrates by ECR assisted

MBE.

GaN films were successfully grown on Si(001) and (111) substrates, using this two-step process. The films on Si(001) are single-crystalline, and epitaxially stabilized in the zincblende structure, while those on Si(111) have the wurtzite structure. Although RHEED suggest that the wurtzitic GaN on Si(111) is single-crystalline, considerable amount of cubic phase was detected by XRD studies, and was attributed to larger concentration of stacking faults along the growth direction.

GaN films were also grown on the c-plane, a-plane, and r-plane sapphire. The growth process involves the conversion of the sapphire surface into AlN by plasma nitridation. The XRD studies indicate that GaN films on the c-plane sapphire have the best crystalline quality.

Acknowledgements

We are grateful to Prof. Karl Ludwig for stimulating discussions and help with XRD studies. This work was supported by the Office of Naval Research (Grant No. N00014-92-J-1436).

References

[1] R. F. Davis, Proceedings of the IEEE., V. 79, No. 5, 702 (1991); R. F. Davis, Z. Sitar, B. E. Williams, H. S. Kong, H. J. Kim, J. W. Palmour, J. A. Edmond, J. Ryu, J. T. Glass and C. H. Carter, Jr., Mat. Sci. & Eng. B1, 77 (1988).

[2] J. I. Pankove, MRS Symposium Proceedings, V162, 515 (1990).

[3] P. Das and D. K. Ferry, Solid State Electron., 19, 851 (1976).

[4] H. P. Maruska and J. J. Tietjen, Appl. Phys. Lett. 15, 327 (1969).

[5] J. I. Pankove, Phys. Rev. Lett., 34, 809 (1975).

[6] R. Madar, G. Jacob, J. Hallis and R. Fruchart, J. Cryst. Growth 31, 197 (1975).

[7] B. Monemar, O. Lagerstedt and H. P. Gislkason, J. Appl. Phys. 51, 625 (1980).

[8] T. Sasaki and S. Zembutsu, J. Appl. Phys., 61, 2533 (1986).

[9] M. A. Khan, R. A. Skogman, R. G. Schulze and M. Gershenzon, Appl. Phys. Lett., 42, 430 (1983).

[10] M. A. Khan, J. N. Kuznia, J. M. Van Hove, D. T. Olson, S. Krishnankutty and R. M. Kolbas, Appl. Phys. Lett., 58, 526 (1991).

[11] M. A. Khan, J. M. Van Hove, J. N. Kuznia and D. T. Olston, Appl. Phys. Lett., 58, 2408 (1991).

[12] M. Manasewit, F. M. Erdmann and W. I. Simpson, J. Electrochem. Soc., 118, 1864 (1971).

[13] H. Amano, N. Sawaski, I. Akasaki and Y. Toyoda, Appl. Phys. Lett., 48, 353 (1986).

[14] T. Kawabata, T. Matsuda and Susumu Koike, J. Appl. Phys., 56, 2367 (1984).

[15] T. Duffy, C. C. Wang, G. D. O'Clock Jr., S. H. McFarelane and P. I. Zanzucchig, J. Electron. Mater., 2, 359 (1973).

[16] H. Gotoh, T. Suga, H. Susuki and M. Kimata, Jpn. J. Appl. Phys., 20, L545 (1981).

[17] S. Yoshida, S. Misawu and S. Gonda, Appl. Phys. Lett., 42, 427 (1983).

[18] M. J. Paisley, Z. Sitar, J. B. Posthil and R. F. Davis, J. Vac. Sci. Tech., 7, 701 (1989).

[19] R. C. Powell, G. A. Tomasch, Y. W. Kim, J. A. Thornton and J. E. Greene, MRS Symposium Proceedings, V162, 525 (1990).

[20] Z. Sitar, M. J. Paisley, B. Yan and R. F. Davis, MRS Symposium Proceedings, V162, 537 (1990).

[21] T. Lei, M. Fanciulli, R. Molnar, Y. He, T. D. Moustakas and J. Scanlon, *Growth of cubic GaN films on Si(100)*, Bull. American Phys. Soc. , 36, 543 (1991).

[22] T. Lei, M. Fanciulli, R. J. Molnar, T. D. Moustakas, R. J. Graham and J. Scanlon, Appl. Phys. Lett., 58, 944 (1991).

[23] T. Lei, T. D. Moustakas, R. J. Graham, Y. He and S. J. Berkowitz, J. Appl. Phys., 71, 4933, (1992).

[24] T. Lei and T. D. Moustakas, Mat. Res. Soc. Proc., Vol. 242, 433 (1992).

[25] T. D. Moustakas, R. J. Molnar, T. Lei, G. Menon and C. R. Eddy Jr., Mat. Res. Soc. Proc. Vol. 242, 427 (1992).

[26] T. P. Humphreys, C. A. Sukow, R. J. Nemanich, J. B. Posthil, R. A. Rudder, S. V. Hattangady and R. J. Markunas, *MRS Symposium Proceedings*, V162, 531 (1990).

[27] E. Lashimi, B. Mathur, A. B. Bhattacharya and V. P. Bhargava, Thin Solid Films, 74, 77 (1980).

[28] S. Zembutsu and T. Sasaki, Appl. Phys. Lett., 48, 870 (1986).

[29] S. Zembutsu and M. Kobayashi, Thin Solid Films, 129, 289 (1985).

[30] J. Knights and R. A. Lujan, J. Appl. Phys., 49, 129 (1978).

[31] J. I Pankove, S. Bloom and G. Harbeke, RCA Rev., 36, 163 (1975).

[32] O. Lagerstedt and B. Monemar, J. Appl. Phys., 45, 2266 (1974).

[33] W. Seifert, R. Franzheld, E. Butter, H. Sobotta, V. Riede, Crystal Res. and Technol., 18, 383 (1983).

[34] H. Amano, M, Kito, K. Hiramatsu and I. Aksaki, Jap. Jour. Appl. Phys., 28, L2112-L2114 (1989).

[35] S. Nakamura, Jpn. J. Appl. Phys., 30, L1705 (1991).

[36] M. Mizuta, S. Fujieda, Y. Matsumoto and T. Kawamura, Japanese J. Appl. Phys. 25, L945 (1986).

[37] S. Strite, J. Ruan, Z. Li, N. Manning, A. Salvador, H. Chen, D. J. Smith, W. J. Choyke and H. Morkoc, J. Vac. Sci. Technol. B9, 1924 (1991).

[38] G. Menon, M. S. thesis, Boston University (1990).

[39] S. N. Basu, private communications.

[40] B. E. Warren, X-ray diffraction, Addison-Welsley Publ. Company, Inc. (1969).

Figure Captions

Figure 1. Schematic of the deposition system.

Figure 2. Magnetic field configuration under optimized growth conditions.

Figure 3. RHEED patterns of Si(001) substrates after the routine preparation. (a) for [100] azimuthal incidence of the electron beam; (b) for [110] azimuthal incidence of the electron beam.

Figure 4. RHEED patterns of a GaN buffer grown at $400°C$ for 10 minutes. (a) for [100] azimuthal incidence of the electron beam; (b) for [110] azimuthal incidence of the electron beam.

Figure 5. Typical RHEED patterns of GaN films on p-type or undoped substrate. (a) for [100] azimuthal incidence of the electron beam; (b) for [110] azimuthal incidence of the electron beam.

Figure 6. The RHEED patterns of a GaN film with smooth surface morphology (a) for [100] azimuthal incidence of the electron beam; (b) for [110] azimuthal incidence of the electron beam.

Figure 7. Surface morphology of a GaN thin film on p-type Si substrate. (a) front view; (b) cross-sectional view.

Figure 8. SEM Surface morphology of a smooth GaN thin film (a) on a p-type substrate; (b) on a n-type substrate.

Figure 9. X-ray diffraction using $Cu - K_\alpha$ radiation of a β-GaN film.

Figure 10. ϕ-scan at $(\bar{1}11)$ for a zincblende GaN film.

Figure 11. RHEED patterns for a GaN film on Si(111) with $[11\bar{2}0]$ electron azimuthal incidence.

Figure 12. $\theta - 2\theta$ scans for a wurtzitic GaN film on Si(111).

Figure 13. ϕ-scan for a wurtzite GaN film on Si(111).

Figure 14. $\theta - 2\theta$ scan at the (002) reflection of cubic GaN grains in GaN on Si(111).

Figure 15. ϕ-scan at the $(\bar{1}11)$ peak of cubic GaN components.

Figure 16. RHEED patterns of the sapphire substrates after exposure to the nitrogen plasma: (a) c-plane, (b) a-plane, (c) r-plane.

Figure 17. RHEED patterns of the GaN-buffer on the various sapphire substrates: (a) c-plane, (b) a-plane, (c) r-plane.

Figure 18. RHEED patterns of the GaN films after growth on the various sapphire substrates: (a) c-plane, (b) a-plane, (c) r-plane.

Figure 19. SEM surface morphology of GaN films grown on various substrates: (a) c-plane, (b) a-plane, (c) r-plane.

Figure 20. $\theta - 2\theta$ XRD of the GaN film on various sapphire susbtrate: (a) c-plane, (b) a-plane, (c) r-plane. The inserts show the corresponding rocking curves.

Figure 21. Epitaxial relationship between GaN and (a) the a-plane of sapphire; (b) the r-plane of sapphire.

ECR ASSISTED MBE

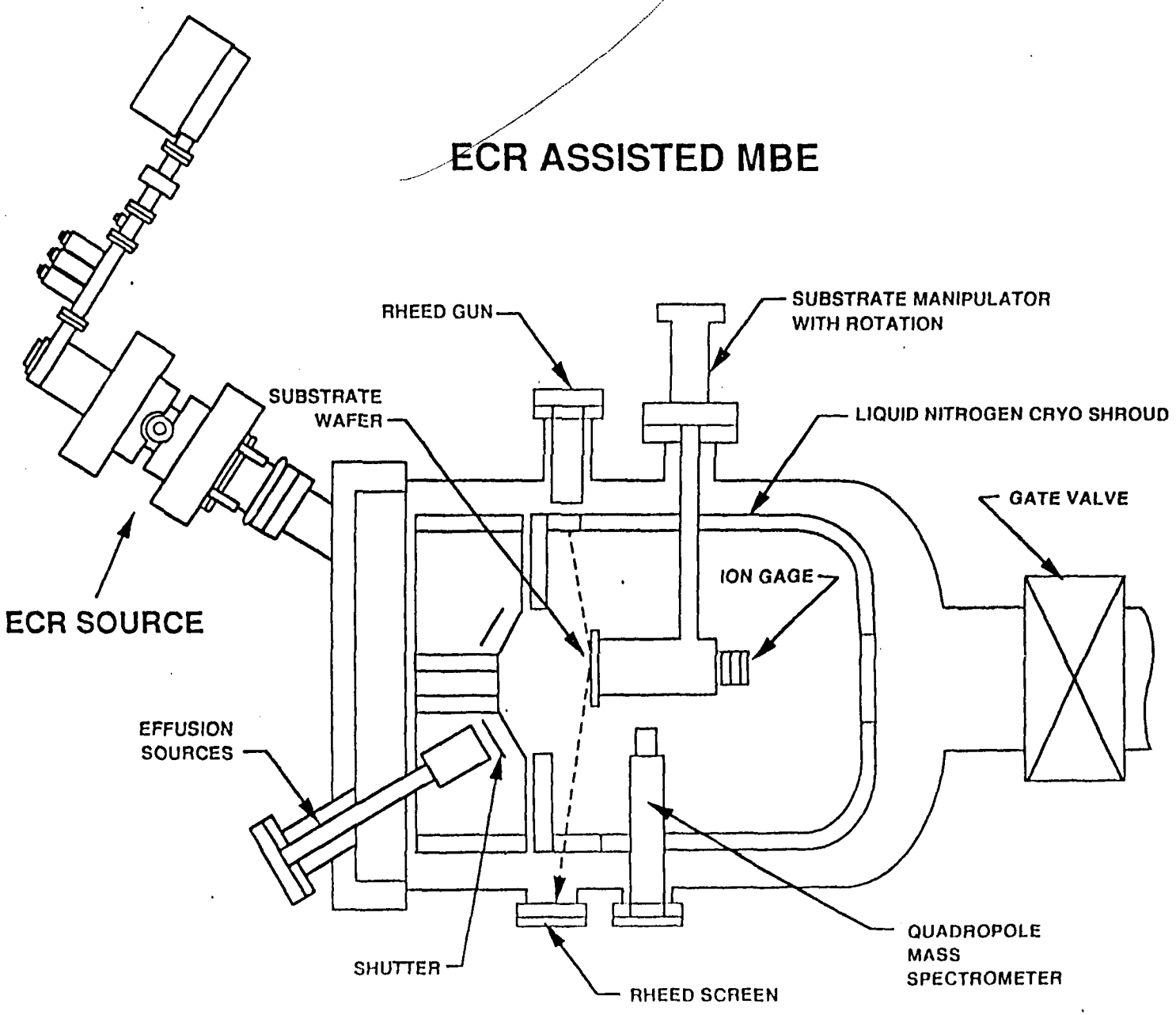

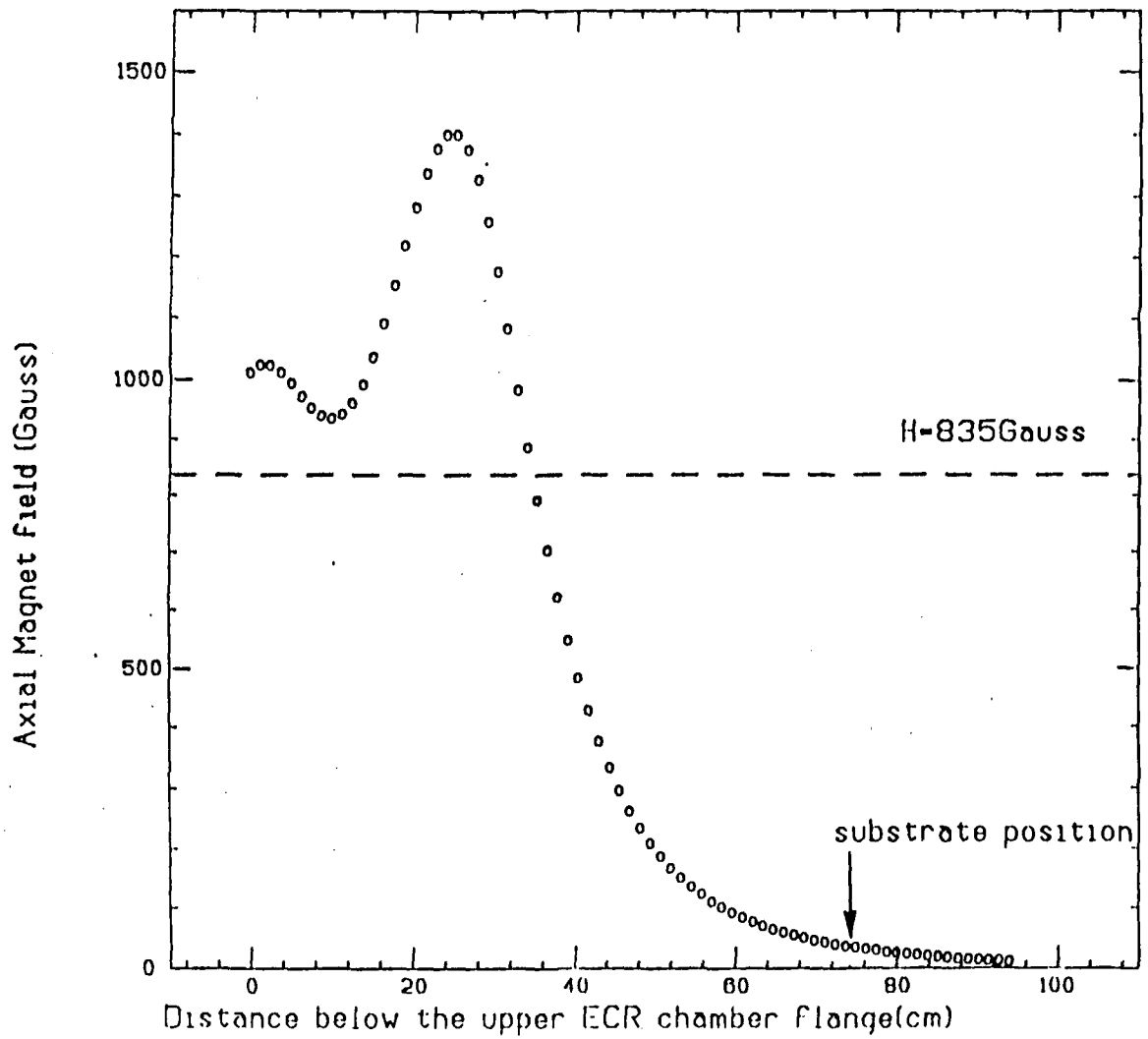
1500
1000
500
0
Axial Magnet Field (Gauss)
H-835Gauss
substrate position
0
20
40
60
80
100
Distance below the upper ECR chamber flange(cm)

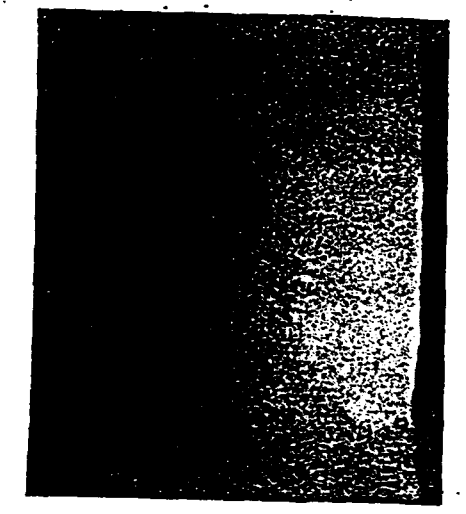

b

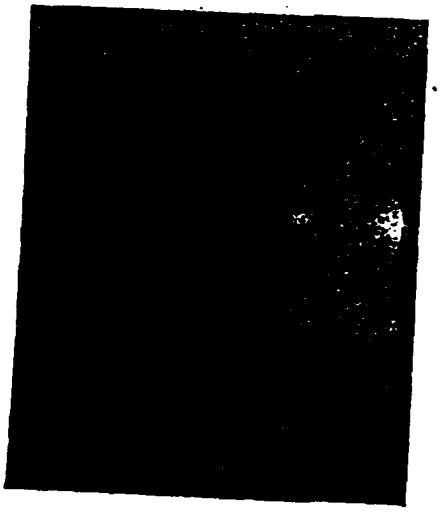

a

Fig 2

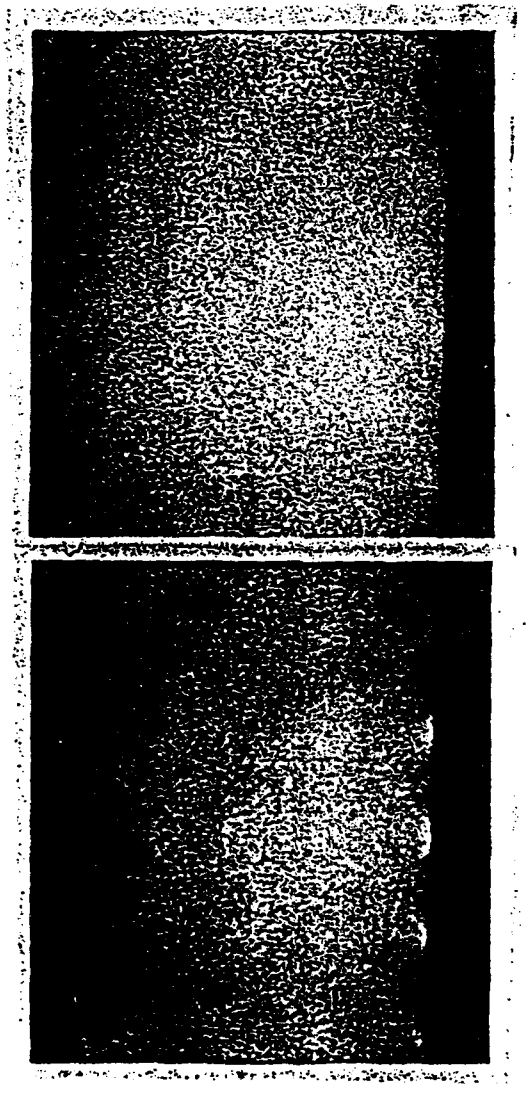

fig 3

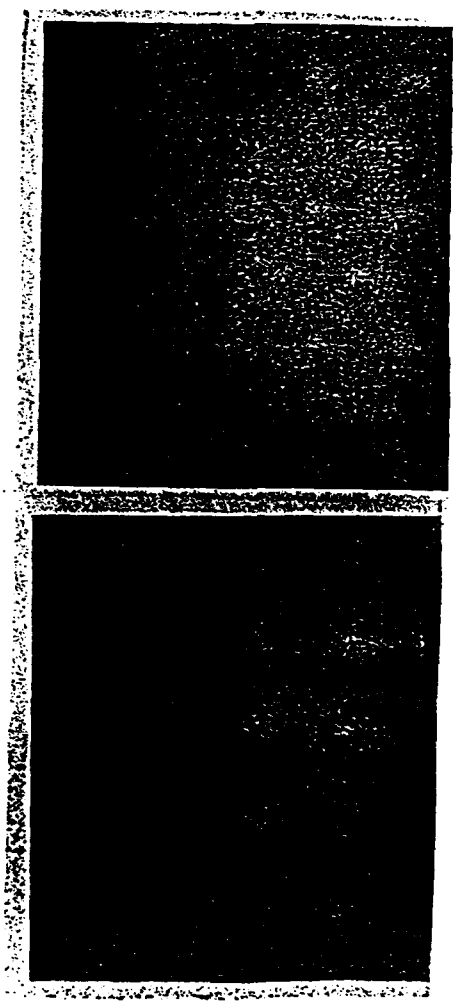

fig 4

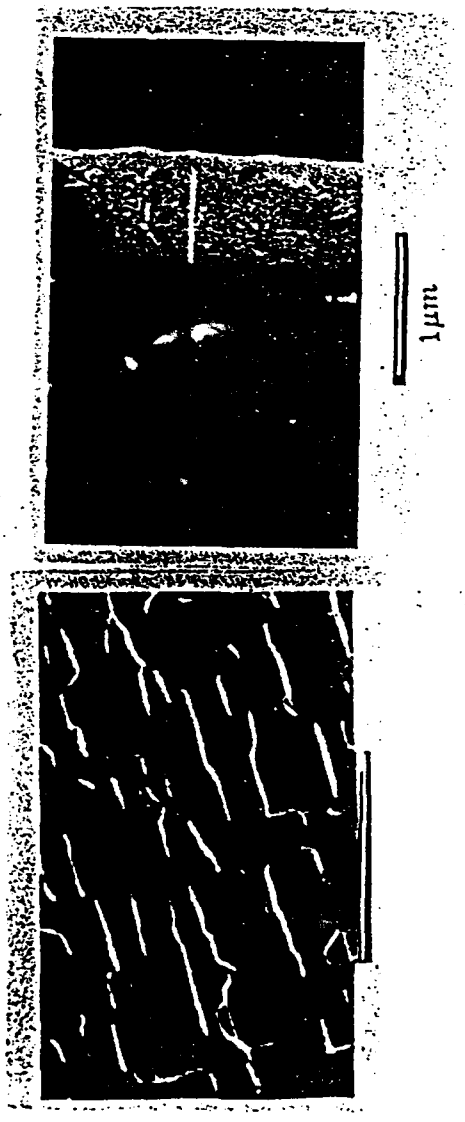

Fig 5

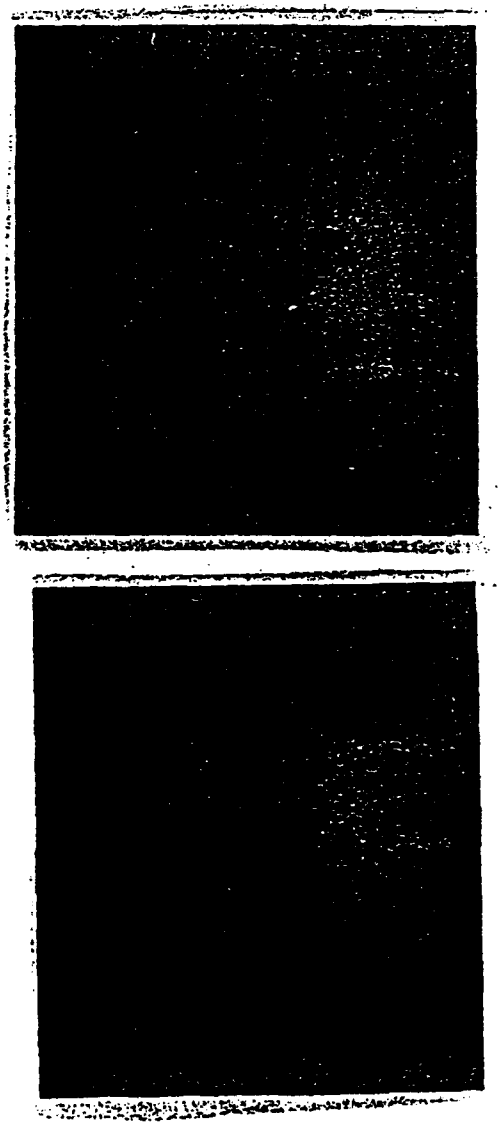

Fig 6

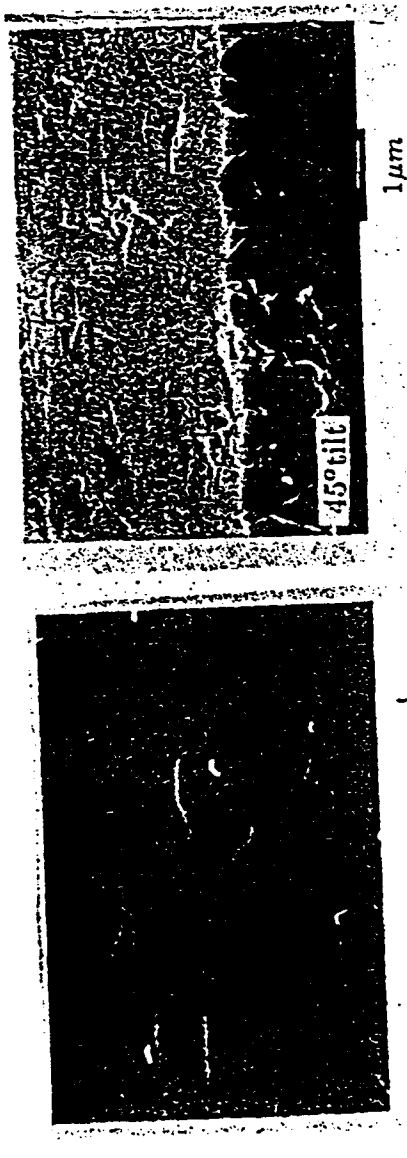

Fig 7

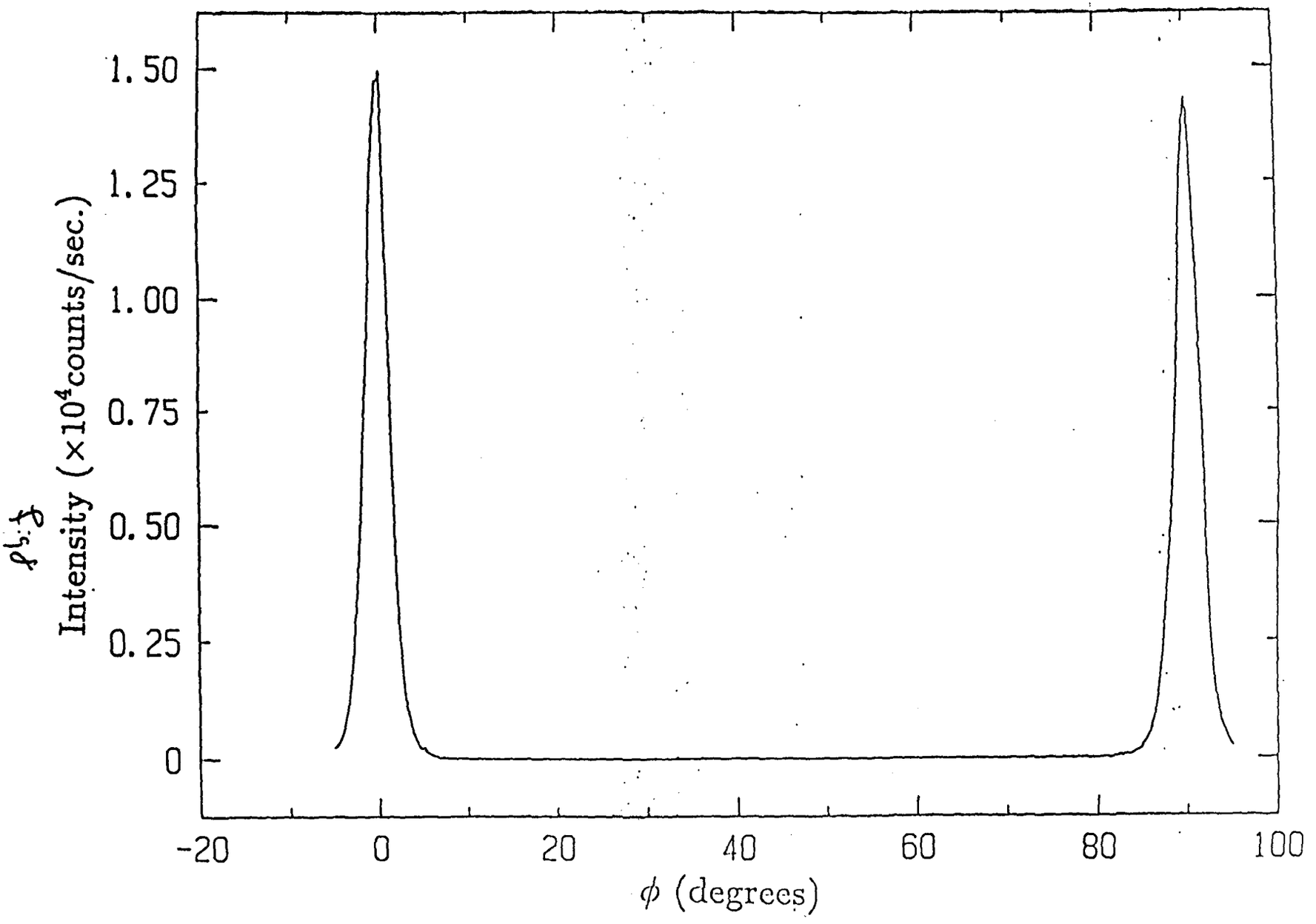
1.50
1.25
1.00
0.75
0.50
0.25
0
Intensity ($\times 10^4$counts/sec.)
-20
0
20
40
60
80
100
ϕ (degrees)

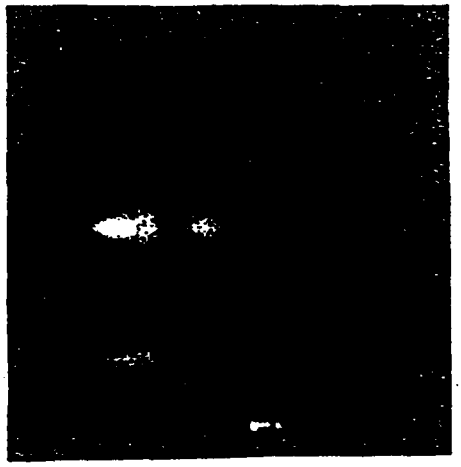

Fig 9

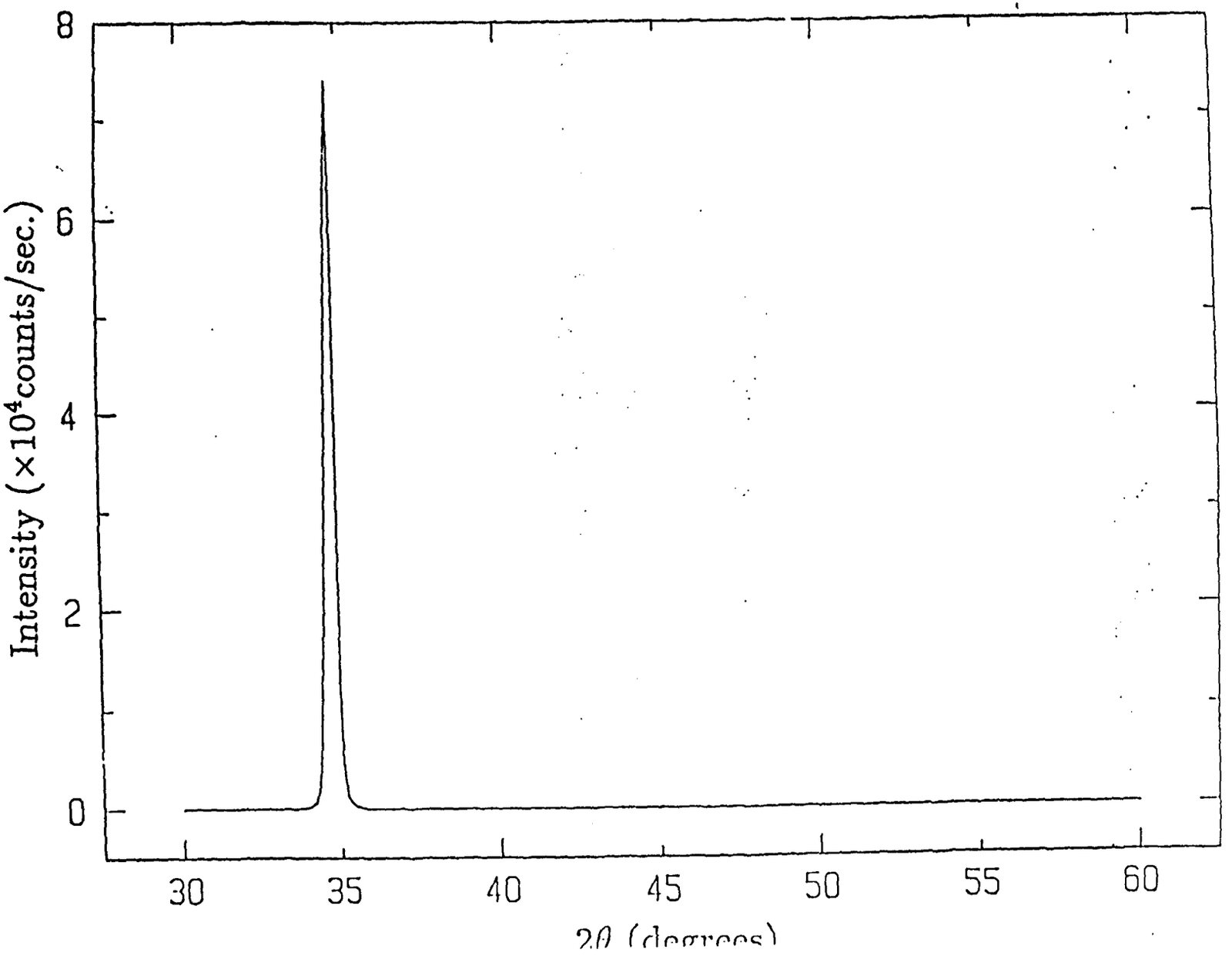
Intensity (×10⁴counts/sec.)
8
6
4
2
0
30
35
40
45
50
55
60
2θ (degrees)

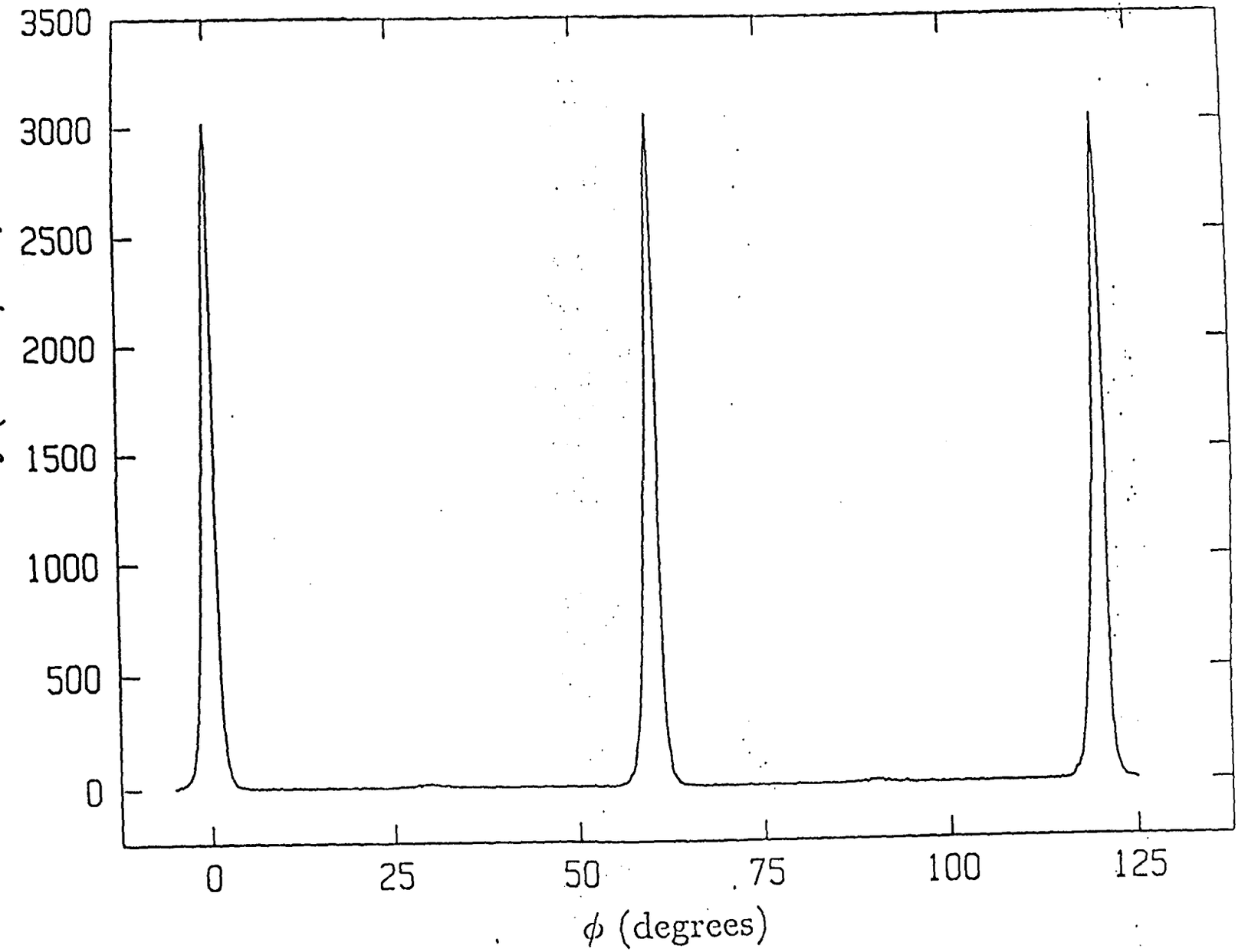
3500
3000
2500
2000
1500
1000
500
0
Intensity (counts/sec.)
0
25
50
75
100
125
ϕ (degrees)

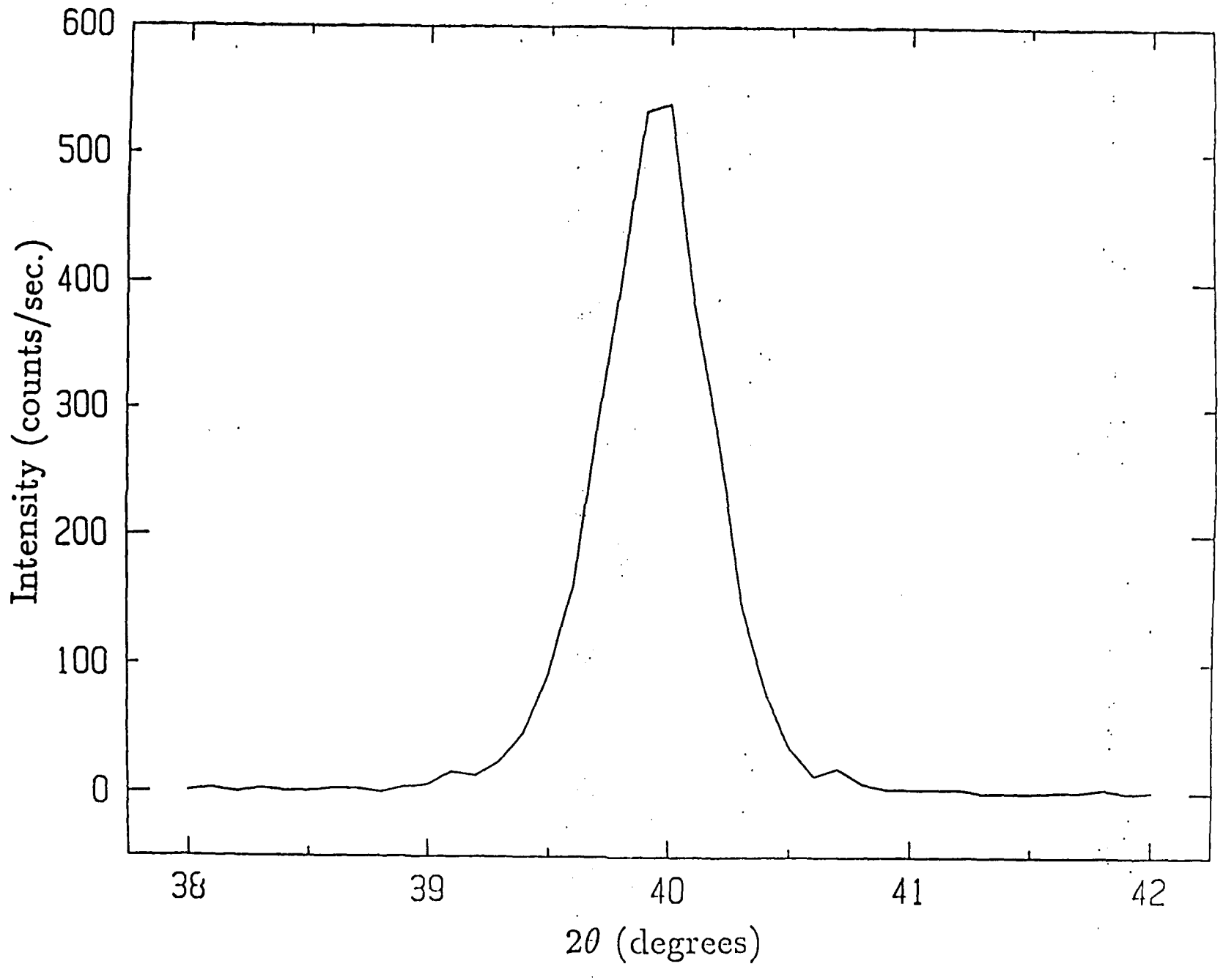
600
500
400
300
200
100
0
Intensity (counts/sec.)
38
39
40
41
42
2θ (degrees)

Fig 12

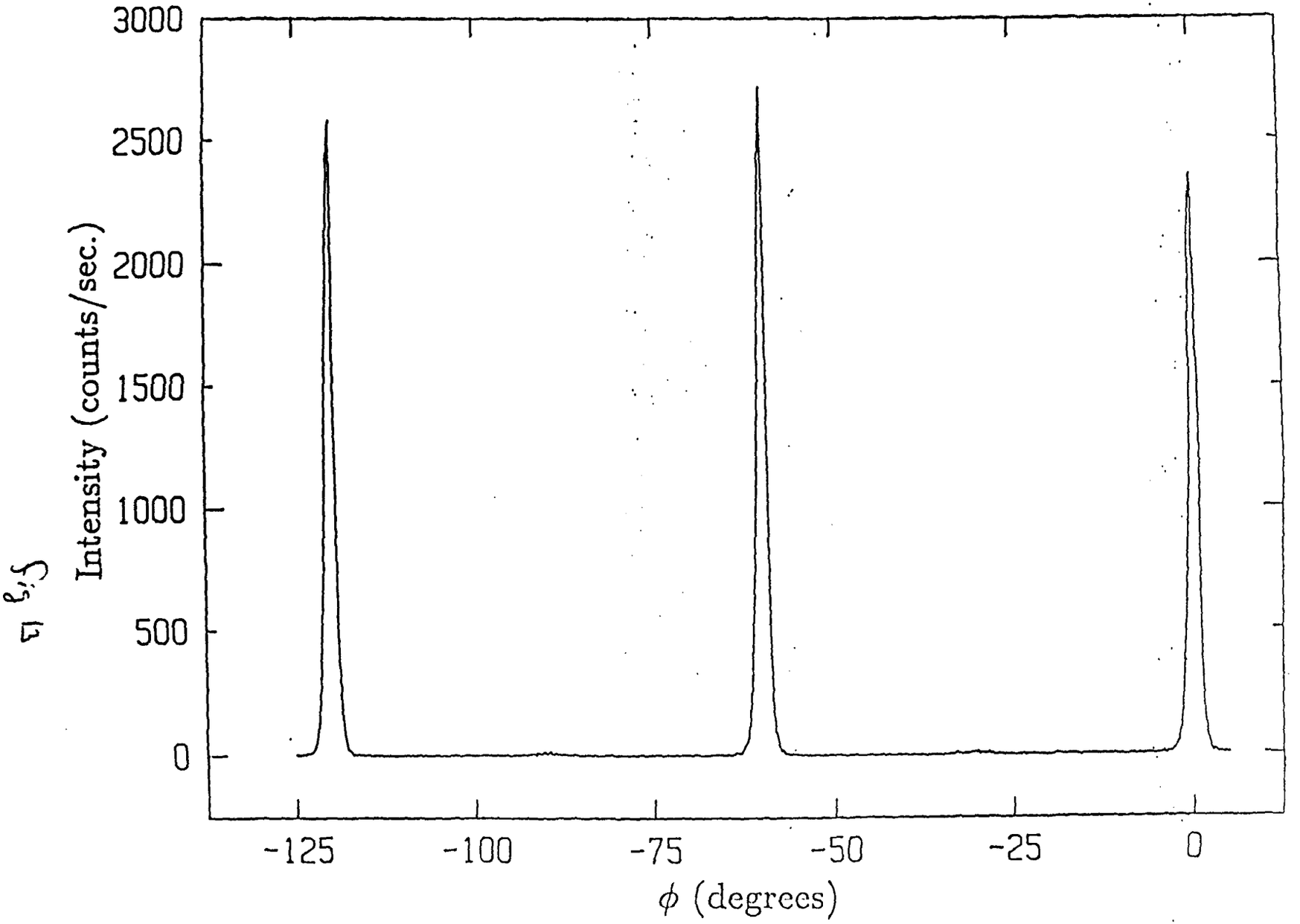
3000
2500
2000
1500
1000
500
0
Intensity (counts/sec.)
-125
-100
-75
-50
-25
0
ϕ (degrees)

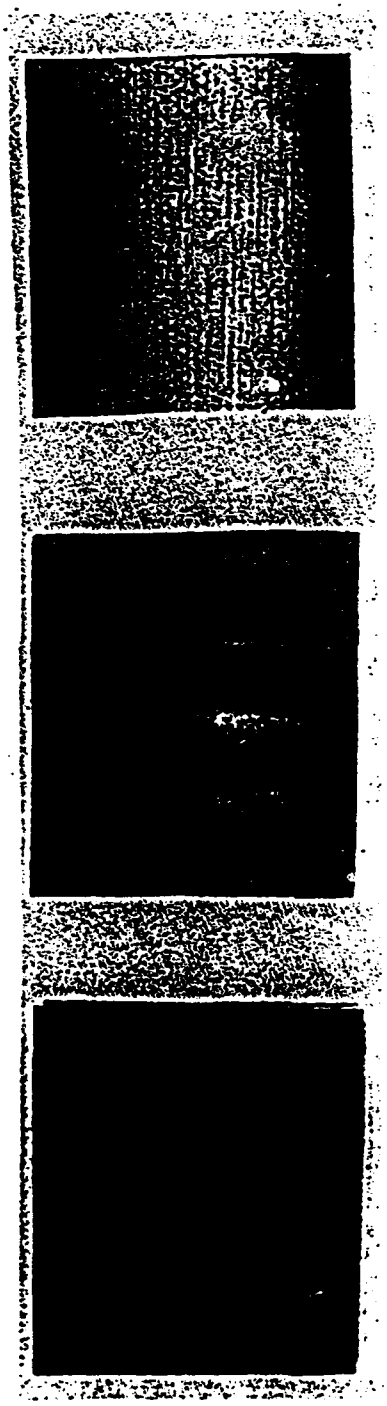

fig 14

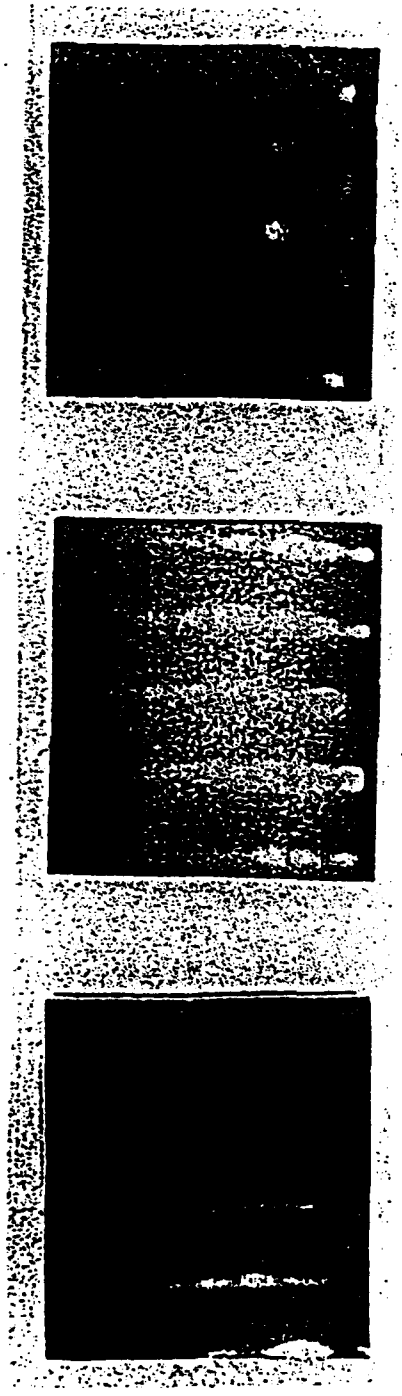

fig 15

fig 1c

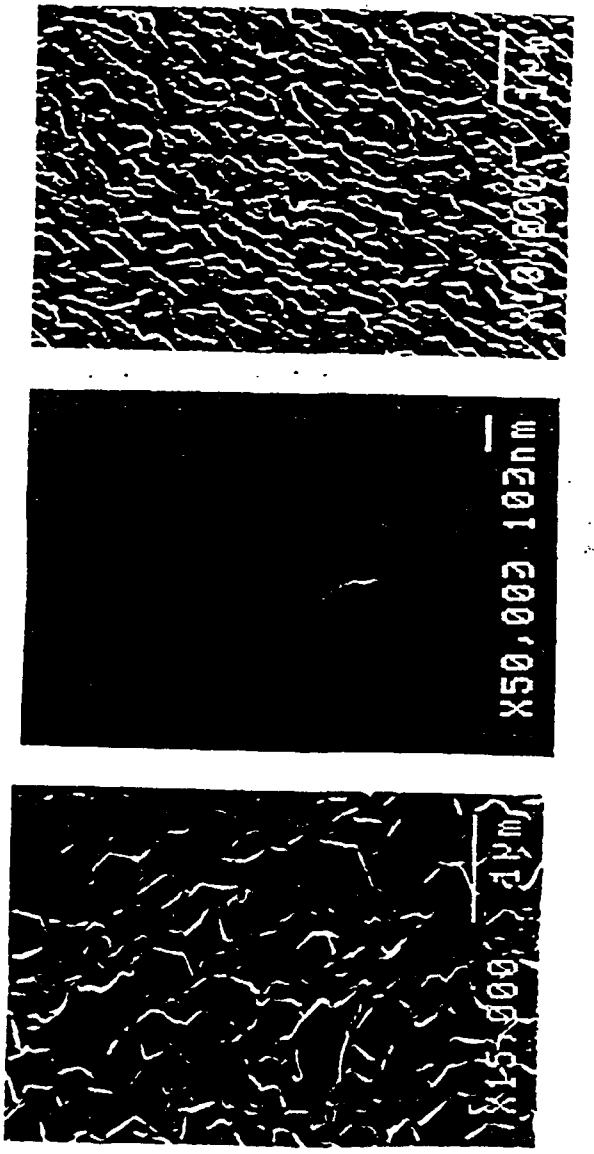

Fig 17

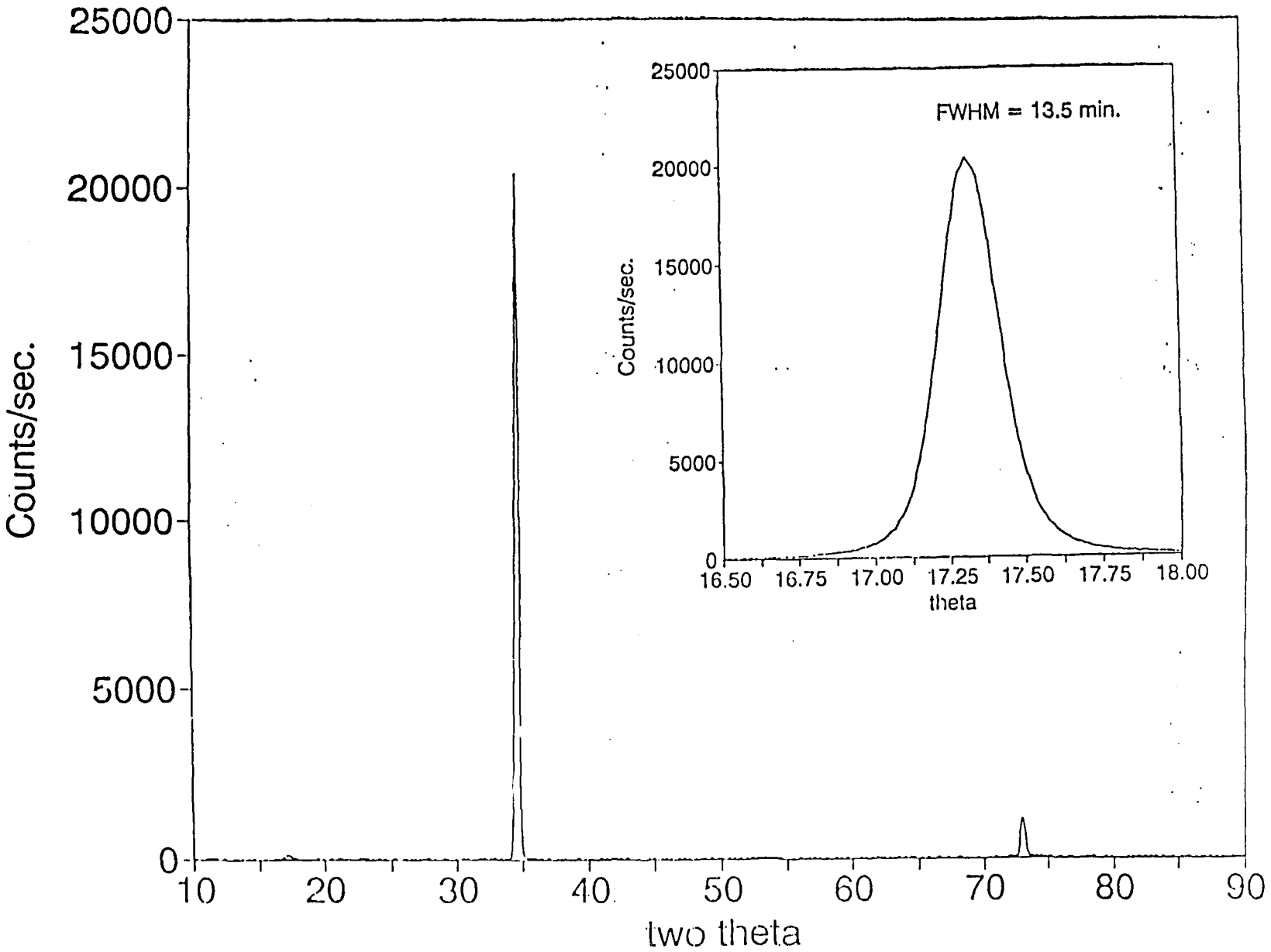
25000
20000
15000
10000
5000
0
Counts/sec.
10
20
30
40
50
60
70
80
90
two theta
FWHM = 13.5 min.
25000
20000
15000
10000
5000
0
Counts/sec.
16.50
16.75
17.00
17.25
17.50
17.75
18.00
theta

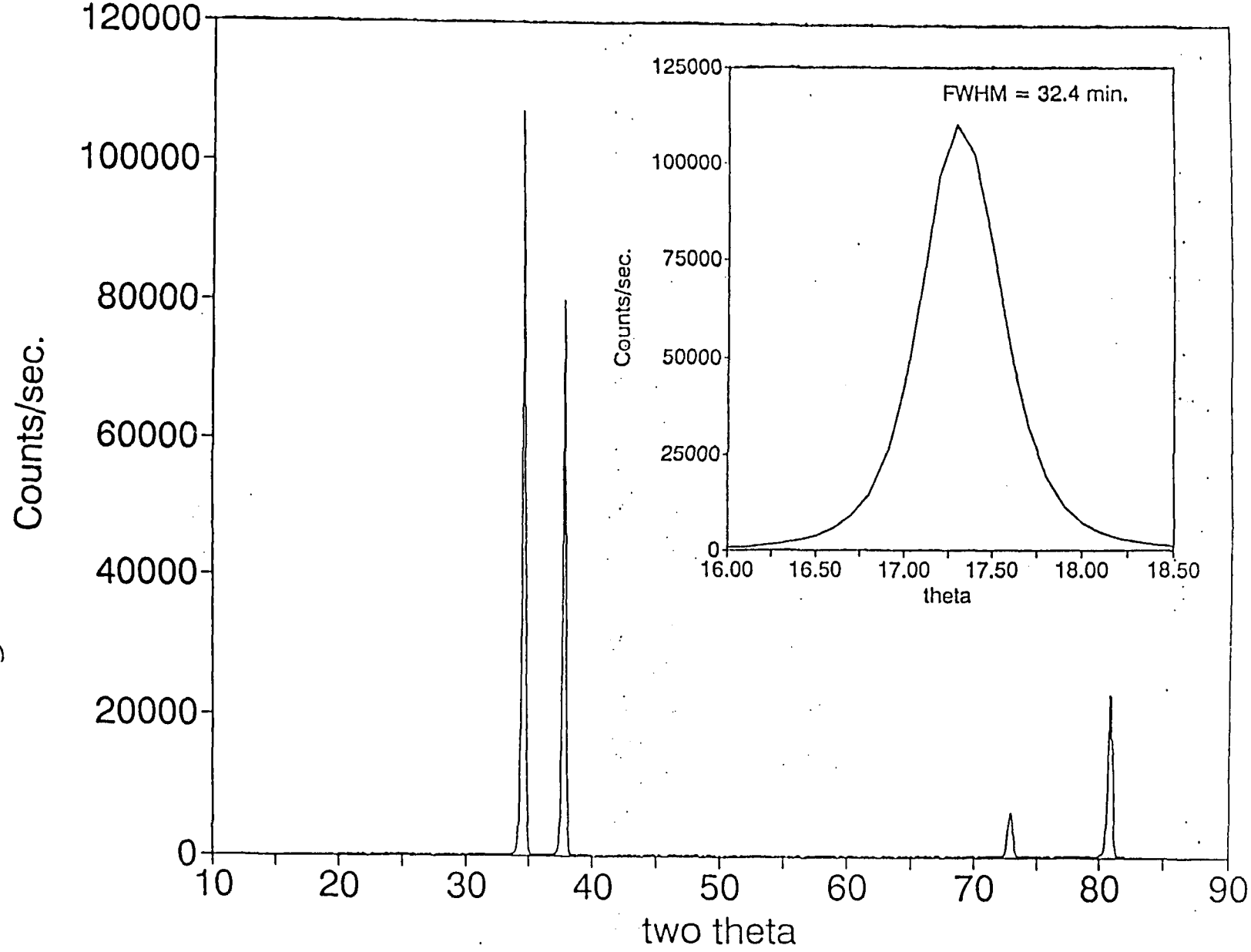
120000
100000
80000
60000
40000
20000
0
Counts/sec.
10
20
30
40
50
60
70
80
90
two theta
125000
100000
75000
50000
25000
0
Counts/sec.
FWHM = 32.4 min.
16.00
16.50
17.00
17.50
18.00
18.50
theta

b

fig 11

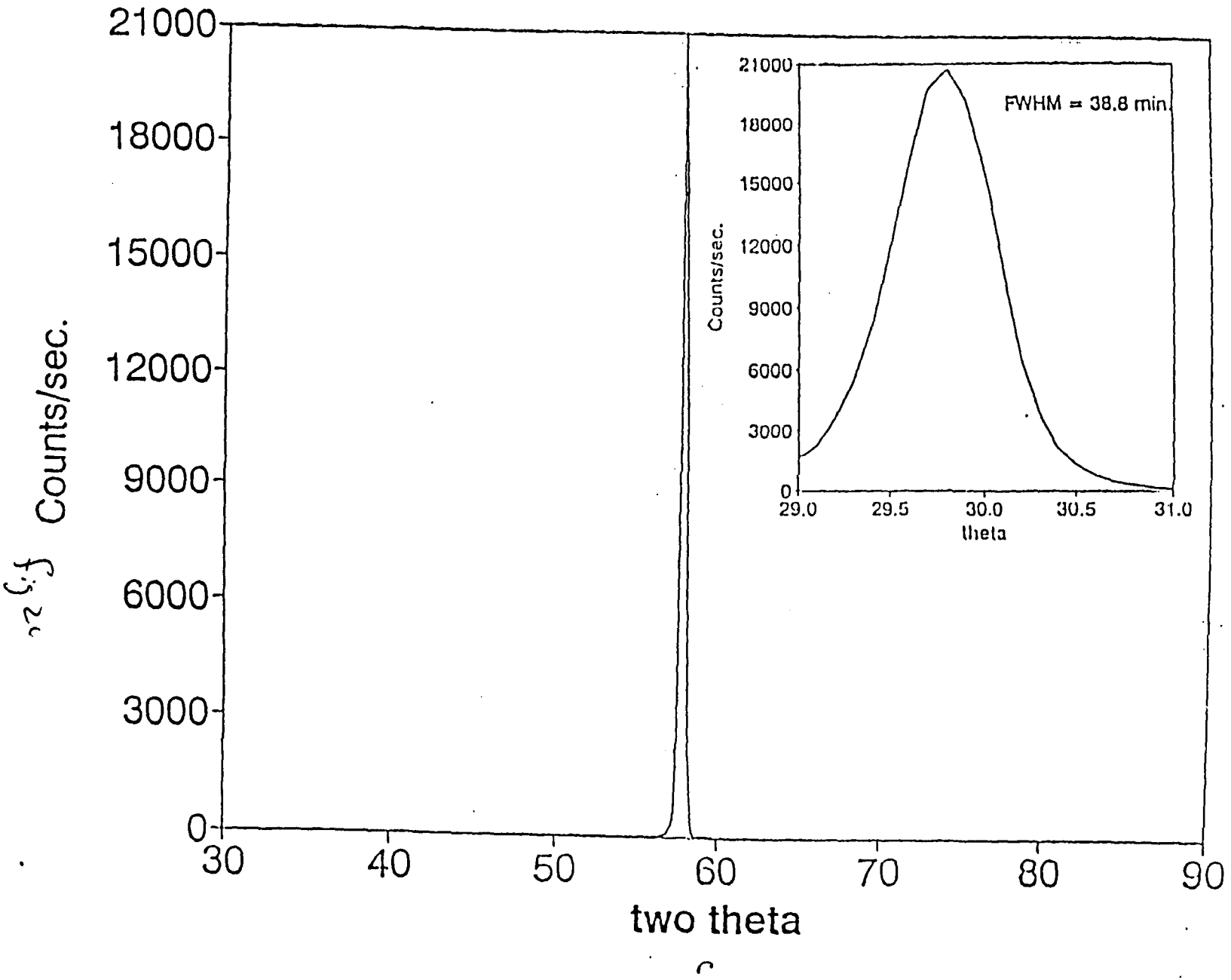
21000
18000
15000
12000
9000
6000
3000
0
Counts/sec.
30
40
50
60
70
80
90
two theta
FWHM = 38.8 min.
21000
18000
15000
12000
9000
6000
3000
0
Counts/sec.
29.0
29.5
30.0
30.5
31.0
theta

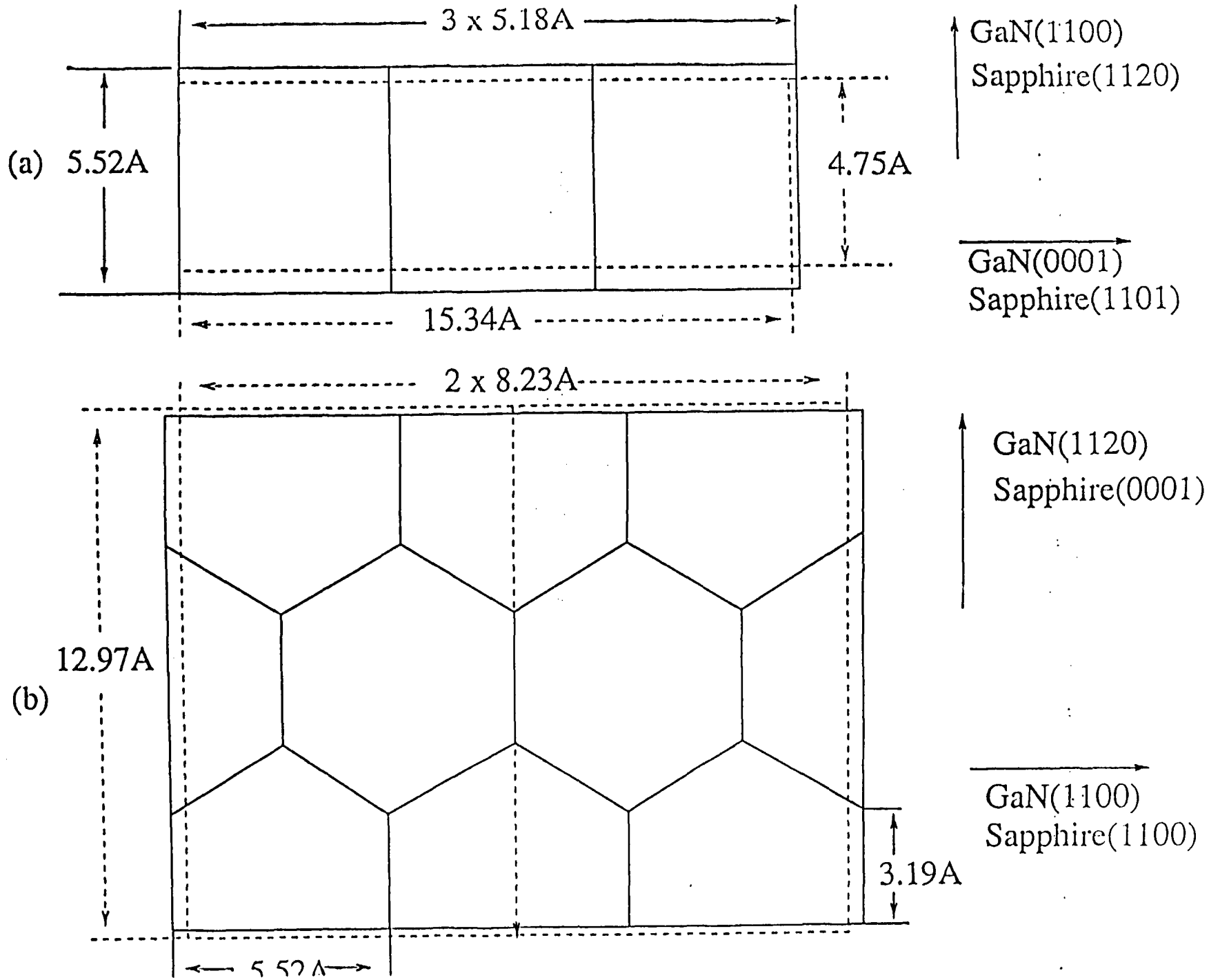
3 x 5.18A
(a) 5.52A
4.75A
15.34A
GaN(1100)
Sapphire(1120)
GaN(0001)
Sapphire(1101)
2 x 8.23A
12.97A
(b)
GaN(1120)
Sapphire(0001)
GaN(1100)
Sapphire(1100)
3.19A
5.52A

Fig 2

Appendix B:

Heteropitaxy, Polymorphism And Faulting In GaN Thin Films on Silicon and Sapphire Substrates

submitted for publication
Journal of Applied Physics

Heteroepitaxy, Polymorphism And Faulting In GaN Thin Films On Silicon And Sapphire Substrates

T. Lei[1]*, K.F. Ludwig Jr.[1] and T.D. Moustakas[1,2]

[1] *Dept. of Physics, Boston University; Boston, MA 02215*

[2] *Dept. of Electrical Engineering, Boston University; Boston, MA 02215*

*Current Address: *Dept. of Materials Science, North Carolina State University*
Raleigh, NC 27695

Abstract:

The structure of GaN films grown by electron-cyclotron-resonance-assisted MBE on Si(111), Si(001), basal-plane sapphire, a-plane sapphire and r-plane sapphire substrates was studied with four-circle x-ray diffractometry. Phase content, domain size, inhomogeneous strain and in-plane and out-of-plane domain misorientations were measured and compared for films grown on each type of substrate. Wurtzite and zincblende polymorphs were found to coexist in films grown on Si(111). The two structures grow in the (0002) and (111) orientations respectively so that they may transform into each other via stacking faults on close-packed planes. Smaller amounts of zincblende material were also found in predominately (0002) wurtzitic films on a-plane sapphire and $(11\bar{2}0)$ wurtzitic films on r-plane sapphire.

1. Introduction:

The growth and properties of GaN films have been under extensive investigation because of their potential applications as light-emitting devices in the blue, violet and near ultra-violet spectra [1,2]. It is known that GaN exists in two polymorphs: wurtzite and zincblende structures with direct bandgaps of 3.4 eV and 3.2 eV respectively. The two are analogous to hcp and fcc structures respectively in their stacking sequences. Since bulk GaN substrates are not available, films must be grown by heteroepitaxy on foreign substrates. The majority of GaN films reported have grown in the wurtzite structure, most commonly with the basal planes parallel to the substrate. However, epitaxial stabilization of the zincblende phase has been obtained on GaAs, MgO, SiC and Si substrates [see the citations in Ref. 1]. All substrates used have a large mismatch to GaN films.

Despite the critical role which substrate symmetry and unit cell size must play in the formation of heteroepitaxial GaN films, relatively little detailed comparative structural work has been performed. While reflective high-energy electron diffraction (RHEED) is often used to characterize films *in situ* [3-6], it probes only the surface structure of the growing film. Electron transmission microscopy (TEM) studies provide important information about the film microstructure and epitaxial orientation [7,8], but they cannot quantitatively examine the degree of orientational order between film domains or reliably detect small phase components. In contrast, x-ray diffraction examines the structure of the bulk of the film, can quantify the degree of film orientational order and can determine oriented minor phase content down to the 10^{-4} level. However, x-ray diffraction measurements limited to Bragg peaks from planes parallel to the substrate have significant limitations. In these cases, experiments cannot distinguish between wurtzitic material in the (0001) and $(11\bar{2}0)$ orientations and zincblende material in the (111) and (110) orientations respectively. Moreover, rocking curves of "on-axis" Bragg peaks [9] show only the orientational order perpendicular to the substrate - they yield no information on the orientational order of film domains in the plane.

We report here a comprehensive x-ray diffraction study examining both the in-plane and out-of-plane structures of GaN films grown by electron-cyclotron-resonance-assisted molecular beam epitaxy (ECR-MBE) on two of the most important substrates for technological applications – silicon and sapphire. Silicon substrates were of (111) and (001) orientation. Sapphire substrates were of (0001) (basal-plane), $(11\bar{2}0)$ (a-plane) and $(1\bar{1}02)$ (r-plane) orientations. The details of the growth process have been previously reported along with brief descriptions of some of the x-ray results [10-13]. All films studied here were approximately one micron thick and included a thin (~ 200 $\mathring{A}$) GaN buffer layer at the substrate interface. We have found that wurtzite and zincblende GaN polymorphs often coexist in films which grow with their close-packed stacking planes parallel to the substrate. This may explain the variable optical and transport measurements sometimes observed in GaN films [14].

2. Experimental Methods:

The x-ray diffraction measurements reported here used Cu K_α radiation in conjunction with a sagitally focussing graphite (002) monochromater crystal for low resolution measurements and a Ge (111) crystal for high resolution work.

The experiments utilized a four-circle diffractometer which allowed access to a large volume of reciprocal space [15]. A schematic of the four-circle geometry is shown in Fig. 1. The horizontal plane M is the one defined by the incident and reflected beams; χ is defined as the angle between the sample surface and plane M and $\chi = 0$ when they are parallel. The angle ϕ measures the rotation around the surface normal of the substrate and 2θ is defined as the angle between the incident and reflected beam. The angle θ measures the sample rotation around the axis perpendiculer to the M plane.

Several different types of scans were utilized to characterize the thin films. The simplest, $\theta - 2\theta$ scans, measure the film structure along the surface normal $\hat{n}$, giving information on phase presence and orientation. Homogenous strain in the film due to uniform

stress or nonstoichiometric composition is reflected in Bragg peak shifts relative to the those expected from measured GaN lattice constants. Inhomogeneous strain and finite domain sizes act to broaden the $\theta - 2\theta$ Bragg peak widths. In reciprocal space, the FWHM width of a peak in a $\theta - 2\theta$ scan includes both effects [16]

$$\delta k = \frac{2\pi}{D} + \epsilon_{in} k, \tag{1}$$

where D is the average domain size and ϵ_{in} is the inhomogeneous strain, i.e. the FWHM variation of the interplanar spacing d through the film, $\delta d/d$. Equation 1 assumes that the peak broadening due to the instrumental resolution has been removed and that the finite domain size and inhomogeneous strain contributions lead to lorentzian peakshapes. Various factors can contribute to ϵ_{in}, including local stresses due to dislocations and mismatch as well as "stress-free" strain due to varying chemical stoichiometry through the film.

As mentioned in the introduction above, $\theta - 2\theta$ measurements do not uniquely determine phase presence and orientation in GaN films because the $(000\bar{2})$ or $(11\bar{2}0)$ planes of wurtzitic GaN films have virtually identical spacings and structure factors as do the (111) and (220) planes of zincblende GaN respectively. Therefore, x-ray diffraction scans at off-axis reflection peaks from planes inclined relative to the substrate were used in this study to distinguish between the wurtzite and zincblende structures. For convenience, we refer to these measurements as $l-$scans if they were performed in the direction of the film normal.

Measurements were also performed to examine the orientational quality of the thin films. Rocking curves of θ around the on-axis Bragg peaks were used to examine the orientational spread of the film parallel to the surface normal. The spread of in-plane orientations as well as the epitaxial relationship between substrate and film axes in the plane were determined with ϕ scans, in which the sample was rotated about its normal while θ, 2θ and χ were held fixed at the peak postion.

3. Experimental Results:

3.1 GaN on Si

A. GaN on Si(111)

X-ray $\theta - 2\theta$ scans of films on Si(111) show only two peaks which are indexed as the wurtzite (0002) and/or zincblende (111) and their harmonic. The peak positions yield a d-spacing of 2.59 $\mathring{A}$, which is consistent with previous lattice constant measurements [1]. No other peaks were observed, ruling out the existence of other epitaxial orientations down to the 0.1% level. Since data from only two peaks are available, the separation of the peak widths into domain size and inhomogeneous strain broadening using Eq. (1) has limited accuracy. However the theta FWHM of the fundamental peak and its harmonic are 0.08° and 0.19° respectively, implying that the dominant contribution to the widths comes from an inhomogeneous strain of approximately 0.2%. The grain size estimated from the peak widths is resolution limited, so that the coherent domain size must be larger than approximately 1500 $\mathring{A}$.

In order to better investigate the polymorph content of the film, l–scans were performed along the wurtzite $(10\bar{1}l)$, $(1\bar{1}0l)$ and $(11\bar{2}l)$ lines in reciprocal space (see Figs. 2 and 3). The scans show that there are significant components of both wurtzite and zincblende phases in the materials. The zincblende further exists equally in its two twins corresponding to ABCABC... and CBACBA... packing. The relative heights of the zincblende and wurtzite peaks suggests that approximately 25% of the film is zincblende and the remainder is wurtzite. The in-plane orientation between the two polymorphs is wurtzite $[10\bar{1}0] \parallel$ zincblende $[1\bar{1}0]$, which is the orientation required in order for the close-packed planes of the two polymorphs to be in registry. It is noteworthy that earlier reports [17] of wurtzite formation on Si (111) could not distinguish between wurtzite and zincblende structures, so that similar polymorph coexistence may have been present there as well.

It is possible that the zincblende and wurtzite phases nucleate independently on the

substrate. However, in cobalt and silicon carbide [18] it is known that the two analogous hcp and fcc polymorphs can nucleate each other at stacking faults on the close-packed planes. Moreover, twinning in metallic crystals as well as in CdTe [19] films can occur in the same way. It is therefore possible that the coexistence of the two polymorphs and of the two zincblende twins in the GaN films may be related to the presence of stacking faults. Approximate fault densities can be obtained from the widths of the off-axis diffraction peaks, since faulting effects the broadening of different reflections unequally. Bragg peaks for which h-k=3n, where n is an integer, are unaffected by faulting along the close-packing planes, while others are broadened in direct proportion to the density of faults [20]. Analysis of the wurtzite $(11\bar{2}4)$ and $(1\bar{1}04)$ peak widths indicates that there is an extra width associated with faulting and implies that the average distance between faults is approximately 800 $\AA$. Although we cannot completely rule out other nucleation mechanisms, TEM studies [21] performed after our initial reports of these results [22] have shown conclusively that wurtzite and zincblende polymorphs do nucleate each other at stacking faults in InN films.

In addition to the peaks which can be indexed to the wurtzite and zincblende structures, there is a very small peak not belonging to these two phases in the $(11\bar{2}l)$ and $(10\bar{1}l)$ scans at l = 1.66 reciprocal lattice units (r.l.u.). The position of a peak at a nonintegral l value suggests that it could be due to a larger superstructure. Polytypes with long repeat periods are well known in the silicon carbide system [18]. However, no other peaks attributable to a long-period polytype are observed and calculations suggest that polytypes would not have a strong reflection at this position. The origin of the peak therefore remains unclear.

The orientational quality of the films normal to the substrate was examined with θ rocking curves at the wurtzite (0002)/zincblende (111) peak (see Fig. 4). The FWHM of the rocking curve, which is a direct measure of the orientational spread of grains around the surface normal, is 0.9°. The orientational quality parallel to the substrate was measured

with ϕ scans at the wurtzite $(1\bar{1}02)$ and zincblende $(\bar{1}11)$ reflections. The dominant peak in the wurtzite $(1\bar{1}02)$ scan has the sixfold symmetry expected from the hexagonal structure. However, very small peaks with slightly less than 1% of the intensity of the dominant peaks were observed at ϕ=30° and ϕ=90°. These indicate that a small fraction of the domains have an in-plane orientation which differs by 30° from the bulk of the wurtzite component. Phi scans of the zincblende $(\bar{1}11)$ show that these 30° misoriented domains exist in that polymorph as well (see Fig. 5). The in-plane orientational spread of the wurtzite film component is 1.9°, twice as large as the out-of-plane orientational spread. The epitaxial in-plane orientation is GaN$[11\bar{2}0]$ || Si$[\bar{1}10]$. This is the same orientation as found in earlier growth studies [17].

B. GaN on Si(001)

We have previously reported the results of $\theta - 2\theta$ scans and rocking curves of GaN films on Si(001) substrates [3,4]. The dominant peaks in the $\theta - 2\theta$ scans are indexed to zincblende (002) and (004). The large widths of the two peaks, 0.40° and 0.72° respectively, indicate a higher inhomogeneous strain and a smaller domain size than occurs on the Si(111) substrate. Application of Eq. (1) yields an approximate inhomogeneous strain of 0.6% and a domain size of 500 $\mathring{A}$.

In addition to the dominant zincblende (002) peak and its harmonic, the $\theta - 2\theta$ scan shows a small peak at the position corresponding to zincblende (111) and/or wurtzite (0002) orientations. Thus approximately 1% of the film has this orientation. Transmission electron microscopy has shown that this component develops in the early stage of the buffer layer deposition.

The rocking curve of the (002) peak is 1.6° wide - much broader than that of GaN on Si(111). The in-plane orientational order of the dominant zincblende (001) phase was examined with a ϕ scan of the (111) reflection. It shows a fourfold rotational symmetry with a spread of approximately 2.5° about the maxima. The ϕ scans show also that the epitaxial relationship between film and substrate is GaN(100) || Si(100).

3.2. GaN on Sapphire Substrates

A. GaN on basal-plane sapphire

As was the case with the Si(111) substrate, the $\theta - 2\theta$ scan of the GaN film on basal-plane sapphire shows two dominant peaks corresponding to wurtzite (0002) and/or zincblende (111) and their harmonic. Again, these values are in good agreement with previously reported values. The widths of the two peaks are 0.06° and 0.11°, from which the grain size is estimated to be greater than 1500$\AA$ and the homogeneous strain to be approximately 0.8%.

In order to further examine the polymorph content of the film, we also searched for $(\bar{1}11)$ reflections of (111) oriented zincblende grains. In contrast to the case for GaN grown on Si(111), however, there is no zincblende (111) intensity down to the 10^{-4} level.

The θ-rocking curve of the film (0002) peak has a FWHM of 0.4°. This is comparable to that observed by Sasaki and Zembutsu [23] in films grown with MOCVD and by Shintani *et al.* [24] using HVPE, but significantly smaller than that in MOCVD films grown on AlN buffers by Amano *et al.* [9]. Phi scans at the $(1\bar{1}02)$ reflection (the off-axis peak) of GaN in the wurtzite structure display the dominant reflection peak as ϕ rotates every 60 degrees, a result of the 6/m symmetry of the rotation axis, as is in the case on Si(111). However, no in-plane misoriented domains were observed. The in-plane orientational spread is 0.8°, about twice as large as the out-of-plane orientational spread. The in-plane orientation of the film is found to be GaN $(11\bar{2}0) \parallel$ sapphire $(1\bar{1}00)$. This is in agreement with previous reports on GaN films on basal-plane sapphire grown by a variety of techniques [3,4,5,6,25]. The lattice mismatch between GaN and the basal plane of the sapphire hexagonal unit cell is over 30%. However, as noted by Kosicki and Kahng [4], the mismatch is significantly less ($\sim$ 15%) between the wurtzite basal plane unit cell and a smaller hexagonal cell within the sapphire unit cell. The smaller cell of Al atoms on the basal-plane sapphire is oriented 30° away from the larger sapphire unit cell, in agreement with the GaN orientation found experimentally. Figure 6 shows that this epitaxial orientation gives relatively good

agreement between the bulk atomic positions Al atoms in the sapphire and Ga ato in the film.

B. GaN on a-plane sapphire

As is the case for GaN grown on Si(111) and basal-plane sapphire, $\theta - 2\theta$ scans of G film on a-plane sapphire show peaks corresponding well to previously published values the wurtzite (0002) interplanar spacing. The FWHM of the two peaks are 0.06° and 0.1 the same as those for GaN on c-plane sapphire, so that the grain size and inhomogene stress are similar. The zincblende $(\bar{1}11)$ peak was examined to measure the percent of (111) oriented cubic phase present. The peak's intensity suggests that approximat 1% of the material has the zincblende structure. A previous examination by Wickenc *et al.* [25] of GaN films deposited by vapor phase epitaxy had reported only the grow of wurtzitic material. It is unclear, however, that the study could distinguish between t wurtzite and zincblende polymorphs.

Although the domain size and inhomogeneous strains of the GaN film grown on plane sapphire are similar to those for films grown on basal-plane sapphire, the θ-rock curve of the film on a-plane sapphire has a FWHM of 0.6°, 50% larger that that of G on basal-plane material. Phi scans at the off-axis wurtzite $(1\bar{1}02)$ reflection show no plane misoriented domains, as is the case with basal-plane sapphire. However, the in-pl orientational spread here is significantly larger - 1.4°. The in-plane epitaxial relationsh was found to be GaN $[11\bar{2}0]$ || sapphire $[1\bar{1}00]$. As Wickenden *et al.* [25] point out, this orientation the bulk positions of the substrate and film cations lie along lines in t sapphire [0001] direction (see Fig. 7). The mismatch between the substrate and film spacings is only ~0.7%, although many of the substrate and film cation positions do n show a good correspondance.

C. GaN on r-plane sapphire

When θ was aligned with respect to the GaN reflection, $\theta - 2\theta$ scans from films grov

on r-plane sapphire showed only a peak which is indexed to the $(11\bar{2}0)$ reflection. No peak from the sapphire substrate was observed. However, when θ was aligned with respect to the substrate reflection, the scan showed only the sapphire $(2\bar{2}04)$ peak. Thus the film planes are not exactly parallel to the $(1\bar{1}02)$ planes of the sapphire substrate. By varying ϕ, it was found that the misorientation is approximately 1.5° and is along the GaN [0001] direction. In order to better measure the phase content of the films, we examined the zincblende (111) off-axis peak. From its peak intensity, we estimate that only $\sim$ 1% of the materials is in the zincblende phase; the remainder is wurtzite. Again, previous studies have reported only the growth of wurtzitic GaN on r-plane sapphire [3,5,22], but it is unclear that they had the ability distinguish between the two polymorphs.

The FWHM of the θ rocking curve at the on-axis peak is 0.6°. This is comparable to values reported by Sasaki and Zembutsu [22] on films grown by MOCVD. In order to examine the in-plane orientation, a ϕ scan was performed at the wurtzite $(1\bar{1}00)$ reflection. The scan shows a repetition every 180° in ϕ, which is a result of the 2-fold symmetry of a-plane GaN. The in-plane orientational spread is 6.7°, the largest for all of the GaN films. Phi scans show that the in-plane orientations between the two film polymorphs and the substrate are wurtzite (0002) $\|$ sapphire $(1\bar{1}01)$ $\|$ zincblende $(1\bar{1}1)$. The wurtzite epitaxial orientation is the same as that found in previous reports of films grown on r-plane sapphire [3,5,22]. Surface studies have found that corundum r-plane surfaces are quite stable and evidently do not significantly reconstruct [26]. It is therefore interesting to note the relatively good agreement between bulk substrate and film cation positions in the experimental epitaxial orientation, as Fig. 8 shows. The lattice mismatch is only 1.3% in the sapphire $[\bar{1}101]$ direction, although it is $\sim$15% in the $[11\bar{2}0]$ direction. The particularly small mismatch in the sapphire $[\bar{1}101]$ direction may be responsible for the small tilt between the GaN planes in the film and the substrate planes. Since the film axis in this direction is slightly longer than that of the substrate, the film planes may tilt up slightly in order to better match the projection of the GaN unit cells onto the interface with

the sapphire unit cells below. Because of the two-fold rotational symmetry of the sapphire r-plane unit cell, however, it is unclear why film domains grow with a misalignment in only one of the two possible directions. An alternate possibility is that the film tilt is related to a miscut of the substrate wafer. However, the tilt was observed in several films and was always oriented along the sapphire [$\bar{1}$101] direction.

4. Discussion and Conclusions:

The results of our four-circle x-ray diffractometry suggest that the coexistence of wurtzite and zincblende polymorphs in GaN thin films may be widespread. As discussed above, most previous studies would not have been able to distinguish between the two, especially if one polymorph exists only at the 1% level. Since the two have different bandgaps and possibly different doping capabilities, it is imperative that future investigators interested in optical and transport properties also evaluate their films' phase contents. For this purpose x-ray or electron diffraction measurements of off-axis Bragg peaks are both suitable, but x-ray diffraction may have somewhat greater sensitivity to small volume fractions and it requires no sample thinning.

To our knowledge, these are the first experiments which have examined the orientational quality of GaN films in the film plane. On all of the films, the range of orientation angles in the plane is 1.5 to 10 times times larger than along the film normal. In-plane misorientations between domains may therefore be the more important in creating domain boundary recombination sites due to broken bonds.

It is noteworthy that the measured film lattice constants in this work are all equal to accepted literature values to within experimental error. Since the lattice paramater is sensitive to the nitrogen concentration [27], this implies that the films' compositions are not too far off stoichiometry. We have, however, observed significant variations in GaN lattice paramaters with varying growth temperature which we attribute partly to the formation of large numbers of nitrogen vacancies [28]. It is widely believed that such

nitrogen vacancies autodope films n-type [1]. The agreement between previously reported lattice constants and those observed here also suggests that the interfacial strain in the films relaxes on length scales significantly smaller than the film thickness. Given the large mismatches present between substrate and film, this is not suprising. For GaN on Si(111) and Si(001) substrates the lattice mismatch is δ=21%. As Figs. 6-8 show, however, films grown on sapphire orient themselves to match the bulk atomic positions of the film and substrate and decrease the effective lattice mismatch below the values for epitaxy on silicon. We note that, in fact, the GaN films do not grow directly on the sapphire substrate surfaces, but rather on very thin AlN layers which grow during the substrate N_2 plasma cleaning process [13]. However, the AlN lattice constant is quite close to that of GaN (3.11 $\AA$ versus 3.19 $\AA$) and our RHEED measurements indicate that the AlN has the same orientation as does the GaN film which grows on top of it. Unfortunately, the detailed structure of the film-substrate interface is unknown so the importance of matching bulk atomic positions in the early stages of film growth is unclear. Despite the reasonably good match of cation positions in the GaN films grown on r-plane sapphire, for example, the orientational spread in the film plane is quite large. Clearly a better understanding of the early growth kinetics and of the interfacial structure would be quite helpful in explaining the epitaxial relationship between film and substrate.

The dominant mechanisms causing the inhomogeneous strains measured in these materials are unclear. Since the films appear to relax quickly to their bulk lattice paramater and are relatively thick, it is unlikely that ϵ_{in} could be dominated by misfit stresses from the substrate interface. However, dislocations introduced to relieve the lattice mismatch could create microstresses which would cause local variations in the lattice constant. While we know of no experimental work relating the GaN bandgap to the lattice paramater, LCAO calculations suggest that the energy matrix elements V which determine the bandgap vary as the inverse square of the separation between atoms [29]. Therefore $\delta V/V = 2\delta d/d$, and a 1% inhomogeneous strain would lead to approximately a 2% variation of the bandgap. This

then could be a significant source of band tailing. Nitrogen vacancies would presumably be the principal mechanism contributing "stress-free" strain due to composition inhomogeneity. While a decrease in nitrogen stoichiometry significantly decreases the wurtzite lattice paramaters [27], we know of no quantitative data relating stoichiometry and lattice constants which would allow us to interpret the inhomogeneous strain in terms of nitrogen deficiencies.

All of the films except those on Si(001) have domain sizes along the surface normal which are larger than our instrumental resolution. The relatively small size of domains in GaN films on Si(001) along with their large spread of in- and out-of-plane orientation angles and relatively large inhomogeneous strain suggest that, structurally, these are the worst films overall. The very large spread of in-plane orientations in the films on r-plane sapphire also implies that there are domain boundaries within the film with a relatively large angle of mismatch. In terms of orientation quality and domain size, then, the best films appear to be those which grow on their close-packed planes. The films on sapphire (0002) substrates are the best of these, with relatively small in- and out-of-plane misorientation and little secondary phase. Despite their orientational quality, however, stacking faults may be common in all of the materials grown in the close-packed orientation. The impact of stacking faults on carrier mobility is unclear. Away from fault edges, their main effect will likely be to cause a local variation in the bandgap. At the fault edges, however, bonds will be broken, producing deep states in the gap. Clearly significant work is required in order to examine the relationship between stacking fault density and electrical properties and to develop approaches which minimize the formation of faults in the growth process.

Acknowledgments

We would like to thank G. Morales and Y. Xie for their help with the x-ray measurements. This work was supported by the Office of Naval Research (Grant No. N00014-92-J-1436).

References

1. R. F. Davis, Proceedings of the IEEE., V. 79, No. 5, 702(1991); R. F. Davis, Z. Sitar, B. E. Williams, H. S. Kong, H. J. Kim, J. W. Palmour, J. A. Edmond, J. Ryu, J. T. Glass and C. H. Carter, Jr., Mat. Sci. & Eng. B1, 77(1988).
2. J. I. Pankove, Mat. Res. Soc. Symp. Proc. 162, 515 (1990).
3. M. Sano and M. Aoki, Jap. J. App. Phys. 15, 1943 (1976).
4. B.B. Kosicki and D. Kahng, J. Vac. Sci. and Tech. 6, 593 (1969).
5. S. Yoshida, S. Misawa and S. Gonda, J. Appl. Phys. 53, 6844 (1982).
6. S. Yoshida, S. Misawa and S. Gonda, Appl. Phys. Lett. 42, 427 (1983).
7. Z. Sitar, M.J. Paisley,, B. Yan and R.F. Davis, Mat. Res. Soc. Symp. Proc. 162, 537 (1990).
8. T.P. Humphreys, C.A. Sukow, R.J. Nemanich, J.B. Posthill, R.A. Rudder, S.V. Hattangady and R.J. Markunas, Mat. Res. Soc. Symp. Proc. 162, 531 (1990).
9. H. Amano, N. Sawaki, I. Akasaki and Y. Toyoda, Appl. Phys. Lett. 48, 353 (1986); I. Akasaki and H. Amano, Mat. Res. Soc. Symp. Proc. 242, 383 (1992).
10. T. Lei, M. Fanciulli, R. J. Molnar, T. D. Moustakas, R. J. Graham and J. Scanlon, Appl. Phys. Lett. 58, 944 (1991).
11. T. Lei, T. D. Moustakas, R. J. Graham, S. J. Berkowitz and Y. He, J. Appl. Phys. 71, 4933 (1992).
12. T. Lei, T. D. Moustakas, Mat. Res. Soc. Symp. Proc. 242, 433 (1992).
13. T. D. Moustakas, R. J. Molnar, T. Lei, G. Menon and C. R. Eddy, Jr., Mat. Res. Soc. Symp. Proc. 242, 427 (1992).
14. T. Lei and T. Moustakas, to be published.
15. W. R. Busing and H. A. Levy, Acta Cryst. 22, 457 (1967).

16. R.W. Vook, in *Epitaxial Growth*, ed. J.W. Matthews (Academic Press, New York, 1975), 339.

17. Y. Morimoto, K. Uchiho and S. Ushio, J. Electrochem. Soc. Solid-State Sci. and Tech. **120**, 1783 (1973).

18. R.W.G. Wyckoff, *Crystal Structures, Vol. 1* (Interscience, New York, 1963), 111.

19. R.D. Horning and J.-L. Staudenmann, Appl. Phys. Lett. **49**, 1590 (1986).

20. B.E. Warren, *X-ray Diffraction* (Addison-Wesley, Reading, 1969), 275.

21. S. Strite, D. Chandrasekhar, D.J. Smith, J. Sariel, H. Chen, N. Teraguchi, and H. Morko, preprint.

22. T.D. Moustakas, T. Lei and R.J. Molnar, Physica B, in press.

23. T. Sasaki and S. Zembutsu, J. Appl. Phys. **61**, 2533 (1987).

24. H. Shintane, Y. Takano, S. Minagawa and M. Mari, J. Electrochem. Soc. **125**, 2076 (1978).

25. D.K. Wickenden, K.R. Faulkner, R.W. Brander and B.J. Isherwood, J. Cryst. Growth **9**, 158 (1971).

26. V.E. Henrich, Rep. Prog. Phys. **48**, 1481 (1985).

27. O. Lagerstedt and B. Monemar, Phys. Rev. B **19**, 3064 (1979).

28. C.R. Eddy, Jr, T.D. Moustakas and J. Scanlon, J. Appl. Phys. **73** (1993), in press.

29. W.A. Harrison, *Electronic Structure and the Properties of Solids* (W.H. Freeman, San Francisco, 1980), 149.

Figure Captions

1. Schematic of the Eulerian four-circle diffraction geometry.
2. Schematic of reciprocal space showing an l-scan along the wurtzite $(10\bar{1}l)$ direction. The dots are allowed wurtzite reflections and the triangles show the allowed zincblende reflections for each of the two twins (primed and unprimed). The off-axis zincblende reflections are labelled with respect to the cubic cell, but the graph units are wurtzite reciprocal lattice units (r.l.u.).
3. An l-scan along the wurtzite $(10\bar{1}l)$ direction. The l reciprocal lattice unit values refer to the wurtzite c-axis and the wurtzite and zincblende peaks are labeled. As discussed in the text, the origin of "peak x" at 1.66 r.l.u. is unclear.
4. A ϕ scan at the wurtzite $(1\bar{1}02)$ peak for a film on Si(111).
5. A ϕ scan at the zincblende $(\bar{1}11)$ peak for a film on Si(111).
6. Projection of bulk basal-plane sapphire and GaN cation positions for the observed epitaxial growth orientation. The dots mark aluminum atom positions and the dashed lines show the sapphire basal-plane unit cells. The open squares mark gallium atom positions and the solid lines show the GaN basal-plane unit cells. The aluminum atoms on the sapphire plane sit at positions approximately 0.5 $\AA$ above and below the plane position.
7. Projection of bulk a-plane sapphire and basal-plane GaN cation positions for the observed epitaxial growth orientation. The dots mark aluminum atom positions and the dashed lines show the sapphire a-plane unit cell. The open squares mark gallium atom positions and the solid lines show the GaN basal-plane unit cells.
8. Projection of bulk r-plane sapphire and a-plane GaN cation positions for the observed epitaxial growth orientation. The dots mark aluminum atom positions and the dashed lines show the sapphire r-plane unit cell. The open squares mark gallium atom positions and the solid lines show the GaN a-plane unit cells.

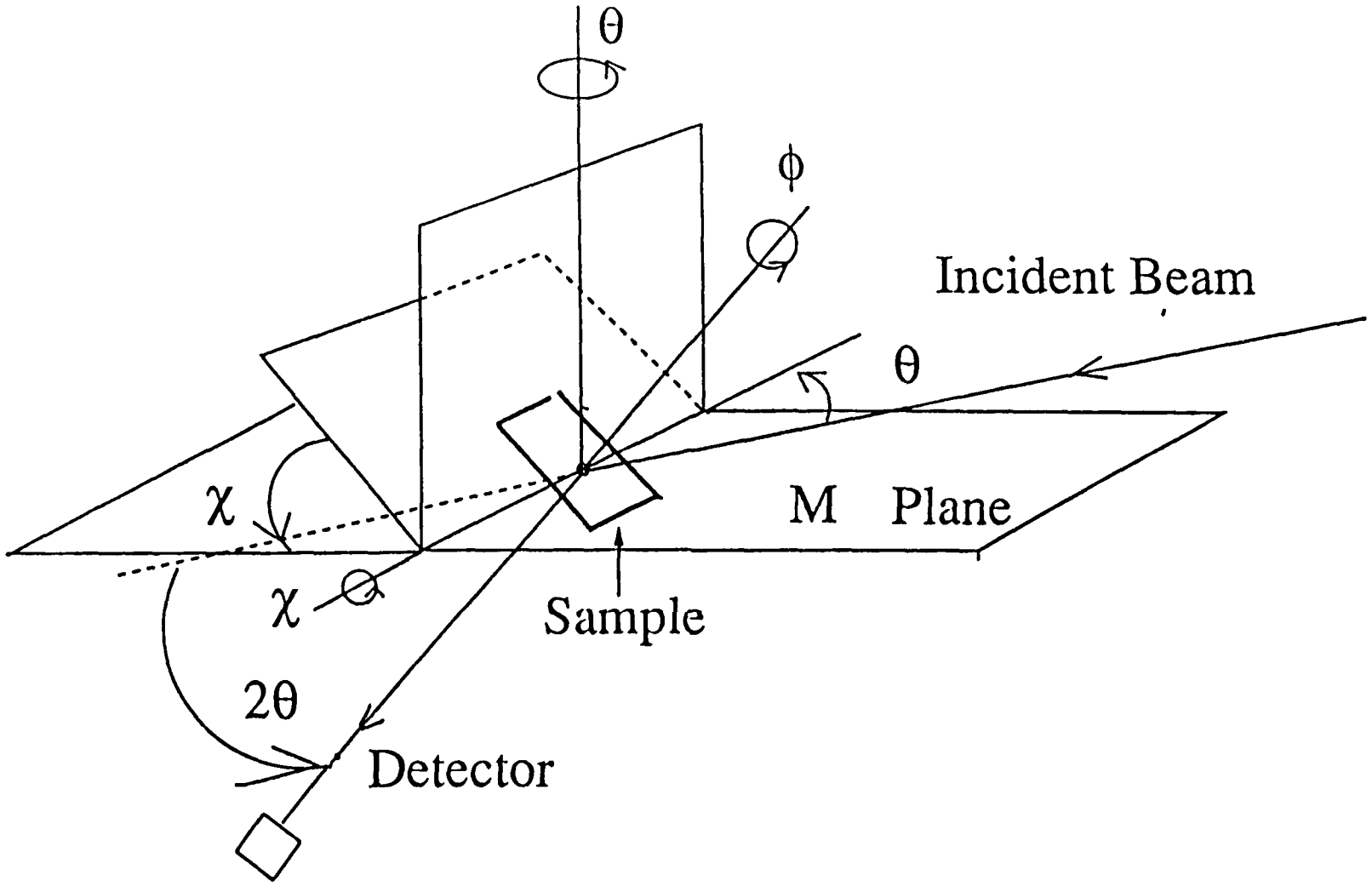

Figure 1

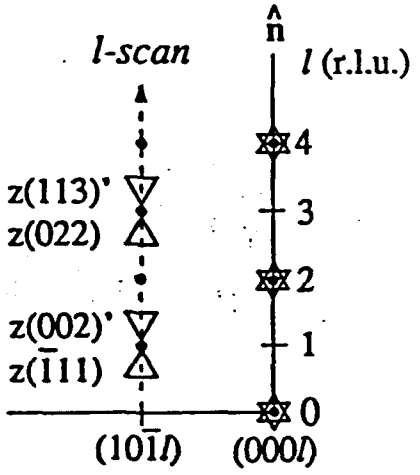

Figure 2

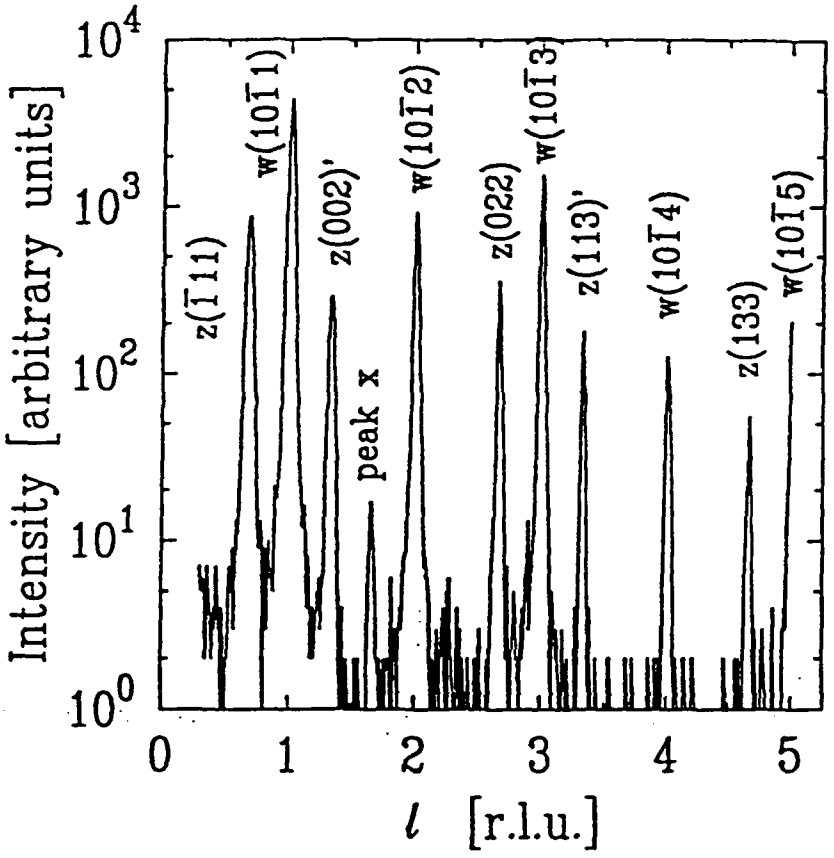
Intensity [arbitrary units]
10^4
10^3
10^2
10^1
10^0
z(1̄11)
w(10Ī1)
z(002)'
peak x
w(10Ī2)
z(022)
w(10Ī3)
z(113)'
w(10Ī4)
z(133)
w(10Ī5)
0
1
2
3
4
5
l [r.l.u.]

Figure 3

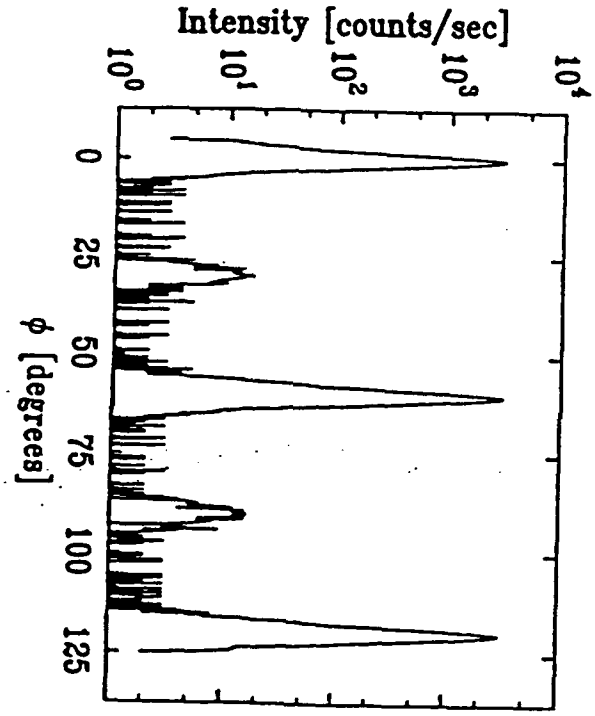
Intensity [counts/sec]
10^0
10^1
10^2
10^3
10^4
0
25
50
75
100
125
ϕ [degrees]

Figure 4

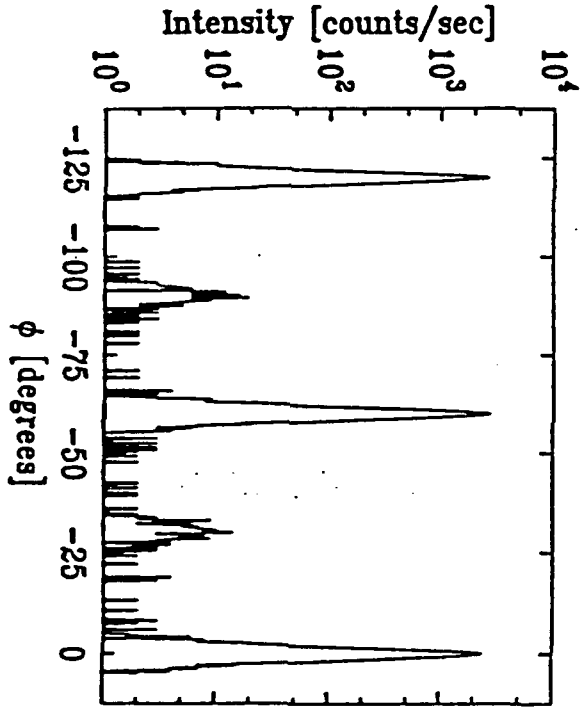
Intensity [counts/sec]
10^0
10^1
10^2
10^3
10^4
-125
-100
-75
-50
-25
0
ϕ [degrees]

Figure 5

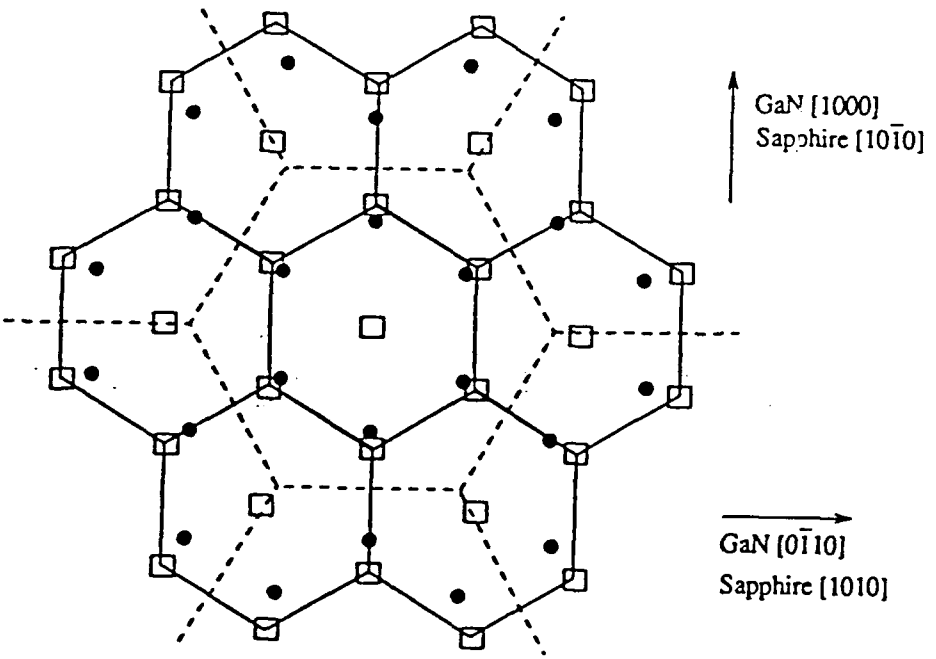

Figure 6

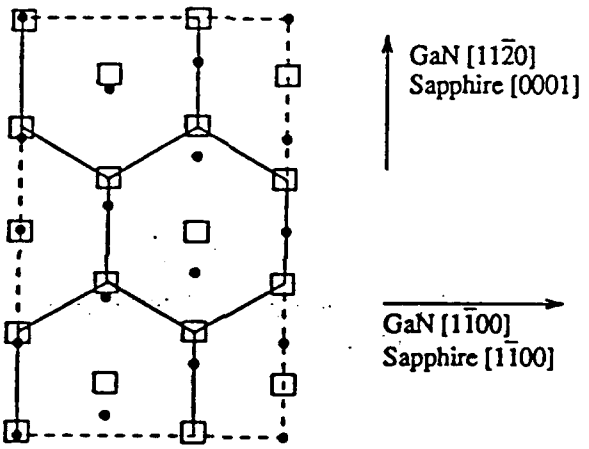

Figure 7

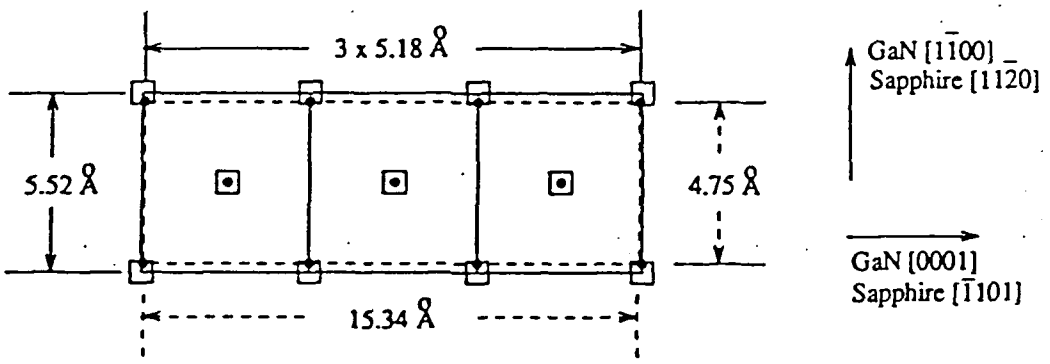
3 x 5.18 Å
5.52 Å
4.75 Å
15.34 Å
GaN [1$\bar{1}$00] _
Sapphire [11$\bar{2}$0]
GaN [0001]
Sapphire [$\bar{1}$101]

Figure 8

Appendix C:

Electron Transport Mechanism in Gallium Nitride

to be published:
Applied Physics Letters, Jan. 1993

Electron Transport Mechanism in Gallium Nitride

R.J. Molnar, T. Lei and T.D. Moustakas

Molecular Beam Epitaxy Laboratory, Department of Electrical Computer and Systems Engineering, Boston University, Boston, MA 02215, U.S.A.

ABSTRACT

The electron transport mechanism in autodoped Gallium Nitride (GaN) films grown by Electron Cyclotron Resonance microwave plasma-assisted Molecular Beam Epitaxy (ECR-MBE) was investigated by studying the temperature dependence of the Hall coefficient and resistivity on samples with various concentrations of autodoping centers. The Hall coefficients go through a maximum as the temperature is lowered from 300 K and then saturate at lower temperatures. The resistivities in the same temperature range initially increase exponentially and then saturate at lower temperatures. These findings are accounted for if a significant fraction of electron transport, even at room temperature, takes place in the autodoping centers and that conduction through these centers becomes dominant at lower temperatures. The activation energy of these centers was found to be on the order of 20-30 meV. When the concentration of the qutodoping centers becomes smaller than that of deep compensating defects, the material becomes semi-insulating and transport by hopping in the compensating defects becomes dominant.

PACS # 72.20.Fr, 72.60.+g, 72.80.-r, 72.80.Ey

Gallium Nitride (GaN) is one of the most promising wide-bandgap semiconductors for the development of high efficiency UV-vis photonic devices due to its direct bandgap. The majority of reported work indicates that the GaN films are autodoped n-type, a result generally attributed to nitrogen vacancies[1,2]. In general, the defect structure of GaN films is poorly understood and very difficult to control experimentally, resulting in difficulties in doping this material p-type[2,3].

GaN films produced by a variety of deposition methods were generally found to have low electron mobilities (<100 $cm^2/V\cdot s$) and high carrier concentration (>10^{18} cm^{-3}) [2,3], although there have been reports[4,5] of mobilities ~600 $cm^2/V\cdot s$ and carrier concentration ~10^{16} cm^{-3}. Some other workers[6,7] reported semi-insulating films. One would expect that more lightly doped films would have higher Hall mobilities. However, such films generally do not have measurable Hall coefficients, suggesting low carrier mobilities,[6,7] while highly conductive (even degenerate) samples readily have mobilities > 20 $cm^2/V\cdot s$. This anomoly has not yet been accounted for.

In this letter, we report on Hall measurements performed on a number of GaN thin films grown on the (0001) plane of sapphire by the Electron Cyclotron Resonance microwave plasma assisted Molecular Beam Epitaxy (ECR-MBE) method. The data is analyzed by taking into account that conduction through defects makes a significant contribution to the electrical transport. The proposed model also accounts for the low mobility in the semi-insulating films.

The films were deposited by the two step growth process in which a GaN buffer is grown first at relatively low temperatures and the rest of the film is grown at higher temperatures[7-12]. This method is capable of producing either conductive or insulating films. The conductive films, which are reported here, are generally grown under conditions (high substrate temperature, low nitrogen overpressure) which are believed to lead to the introduction of nitrogen vacancies[1,2]. These films tend to be covered at the end of the run with microscopic Ga droplets, due to phase separation of excess Ga in the GaN films. To study the transport properties in these films the Ga droplets are etched by emersing them in concentrated HCl. The insulating films, which are grown at high nitrogen overpressure are free of Ga droplets.

The structure and surface morphology of these films were reported elsewhere[10]. X-ray diffraction studies indicate that the films are high-quality single crystals with full width at the half maximum of the θ-rocking curves found to be ~10-20 min.

The films were grown at a deposition rate of 0.2 μm/h and were 1-2 μm thick. The samples were abrasively etched into Van der Pauw lamilla and ohmic contacts were made by annealing

Indium pads. The transport coefficients were measured from 10 K to 300 K in a closed loop helium cryostat. The magnitude of the magnetic field was varied up to 7 kG and the current through the sample was varied from 10^{-5} to 10^{-3} A.

The resistivities of the investigated samples at 300 K are shown in Table I. All the samples are n-type and their room temperature resistivities vary from 0.01 to 0.12 Ω· cm. Figure 1 shows the Hall coefficient vs. 1/T for the investigated samples. For the more resistive samples (118, 119, 110, 115) the Hall coefficient goes through a maximum. The temperature at which this maximum occurs is higher for samples with lower resistivity. In fact, for the least resistive sample (114), the maximum should occur at temperatures above 300 K. The Hall coefficients for all the samples saturate to constant values at low temperatures. The resistivity vs 1/T of the investigated films is shown in figure 2. In all samples the resistivity initially increases as the temperature is lowered and then saturates at a constant value.

Table I - Room temperature resistivities of the investigated samples

Sample	thickness [μm]	Type	Resistivity @ 300 K [Ω· cm]
118	1.9	n	0.121
119	1.7	n	0.074
110	1.8	n	0.038
115	1.8	n	0.025
114	1.1	n	0.012

The observed decrease in the Hall coefficient at low temperatures is not typical for semiconductors[13]. A similar temperature dependence of the Hall coefficient has been reported for GaN films grown by chemical vapor deposition[14] and metalorganic chemical vapor deposition[15]. Ilegems et. al.[14] model the high temperature behavior by assuming two independent donor bands contributing carriers to the conduction band. However, their model does not explain the observation at low temperatures of a decrease in the Hall coefficient, resulting in a large deviation of their fitting from the experimental data at low temperatures. A similar observation was reported earlier for

p-type and n-type Ge[16], where a model involving transport in both the defect centers and the conduction band was introduced to explain the phenomenon. The conduction in the defect centers may be either diffusive, due to the small but finite overlap of the localized electron wavefunctions of the defect centers or hopping[17]. Therefore the defect band mobility is expected to be small compared to the conduction band mobility, and defect band conduction only becomes dominant when carriers in the conduction band become negligible.

The results of Figs. 1 and 2 can be fitted to such a two band model in order to determine the relative concentration and the corresponding mobilities of electrons in the autodoping centers and the conduction band. Let us assume that the donor concentration in our films is N_d, with an activation energy ΔE_d, and that the concentration of deep compensating centers (due to defects such as dislocations) is N_a. At a given temperature, a portion of the net carrier concentration (N_d-N_a) is excited into the conduction band and has mobility μ_c and concentration n_c. The unexcited carriers remain in the defect states with a much lower mobility μ_d and concentration n_d. The net carrier concentration of the conducting carriers is:

$$N_o = n_c + n_d = N_d - N_a \tag{1}$$

Taking both these conduction mechanisms into account, the Hall coefficient, R_H can be expressed as[16]:

$$R_H = \frac{n_c \mu_c^2 + (N_o - n_c)\,\mu_d^2}{(n_c \mu_c + (N_o - n_c)\,\mu_d)^2 e} \tag{2}$$

and the measured resistivity is

$$\rho = \frac{1}{\sigma} = \frac{1}{n_c e \mu_c + (N_o - n_c)\, e \mu_d} \tag{3}$$

Letting $b = \mu_d/\mu_c$, we have

$$eR_H = \frac{(1-b^2)\, n_c + N_o b^2}{((1-b)\, n_c + N_o b)^2} \tag{4}$$

$$\rho = \frac{1}{\mu_c ((1-b) n_c + N_o b) e} \qquad (5)$$

Note that if n_c is much larger than n_d (the high temperature limit), or $\mu_d = 0$ (the defect states do not conduct) the expression for R_H reduces to the expression used for one band conduction. However, for $\mu_d \neq 0$, as the temperature is lowered the carriers in the conduction band will decrease to the point where conduction through the defect states will dominate. It is also apparent from Eqn.(4) that eR_H at both temperature limits is the same and equal to $1/N_0$. If b is not a strong function of temperature, it can be shown that eR_H in Eqn.(4) has a maxima

$$eR_{H_{max}} = \frac{(1+b)^2}{4N_o b} \qquad (6)$$

when

$$n_c = \frac{N_o b}{(1+b)} \qquad (7)$$

Therefore, the expression of R_H in Eqn.(4) qualitatively predicts the shape of the experimental curves shown in Figure 1.

The parameters μ_d, μ_c n_c and n_d are related to R_H and ρ by equations (4) and (5). However, at each temperature, there are three unknowns for the two equations. Hung et. al.[16] approached the problem by assuming that the measurements at high temperatures were dominated by the conduction band electrons and extrapolated the carrier concentration curve to low temperatures to predict n_c at low temperatures. However, we found that in our case, the defect band conduction is not negligible even at room temperature and therefore we did not adopt this approach.

In the case of a well defined activation energy ΔE_d, the carrier concentration in the conduction band is expected to change exponentially with temperature. The parameters N_0, ΔE_d, and μ_c, μ_d at each temperature can be extracted using equations (4)-(7) [12]. The extracted values of N_0 and ΔE_d for each of the samples are listed in Table II.

Figure 3 shows the temperature dependence of μ_c and μ_d calculated for sample 119. The temperature dependence of μ_c is typical of semiconductors. The scattering is dominated at low temperatures by ionized impurities and at high temperatures by phonon scattering. The temperature

dependence of μ_d is typical of hopping conduction. It should be pointed out that b in all the samples we analyzed (118,119,110,115) is almost constant in the temperature range where the Hall coefficient shows a maximum. This is self-consistent with the previous assumption in the derivation of eq. (6) and (7). Figure 4 shows the temperature dependence of n_c and n_d calculated for the same sample (119). Note that for this sample even at room temperature $n_d \sim n_c$.

Table II - Values of N_0 and ΔE_d for samples studied

Sample	N_0 [carrier/cm^3]	ΔE_D [meV]
118	4.75×10^{17}	19.09
119	5.80×10^{17}	18.82
110	4.00×10^{18}	32.16
115	5.56×10^{18}	31.31
114	2.19×10^{19}	-

The proposed model can also account for the observed degradation in the mobility of semi-insulating GaN film[6,7]. Consider two GaN samples grown under identical conditions except for the incorporation of donors. A sample which is moderately doped will have enough carriers to fill any deep states, known to exist in GaN films[18], and additional carriers may be thermally excited into the conduction band. These carriers can generally have quite high mobility and, if their concentration is significant, will easily dominate the electrical properties of the material, i.e. giving the observed high mobilities. However, if the concentration of donors is smaller than the deep defects, the material will be fully compensated with its Fermi level pinned by these defects. In such a material, transport is dominated by hopping in the compensating centers leading to low electron mobilities.

In conclusion, we studied the transport mechanism of a number of GaN films produced by the ECR-MBE method. The experimental results were accounted for by invoking conduction both through the conduction band and the autodoping centers at 20 to 30 meV below the conduction band. When the concentration of the autodoping centers becomes smaller than the deep compensating defects, the material becomes semi-insulating and the transport is determined by electron hopping through the deep compensating defects. This accounts for the low electron

mobility of the semi-insulating GaN films. The nature of the autodoping centers is assumed to be nitrogen vacancies, and their energy levels are found to be 20-30 meV. The compensating defects are assumed to be due either to impurities or dangling bond related defects in dislocations.

We would like to thank M. Yoder for his encouragement in this effort. This work was supported by the Office of Naval Research (Grant No. N00014-92-J-1436).

1. H. P. Maruska and J. J. Tietjen, Appl. Phys. Lett. **15**, 327 (1969).
2. J. I. Pankove, MRS Symp. Proc., **162**, 515 (1990).
3. R. F. Davis, Proc. IEEE., **79**, 702 (1991).
4. M. Ilegems, J. Cryst. Growth **13/14**, 360 (1972).
5. S. Nakamura, Jpn. J. Appl. Phys. **30**, L1705 (1991).
6. R.C. Powell, G.A. Tomasch, Y.W. Kim, J.A. Thornton and J.E. Greene, MRS Symp. Proc., **162**, 525 (1990).
7. G. Menon, MS Thesis, Boston University (1990).
8. T. Lei, M. Fanciulli, R. J. Molnar, T. D. Moustakas, R. J. Graham and J. Scanlon, Appl. Phys. Lett., **59**, 944 (1991).
9. T. Lei, T. D. Moustakas, R. J. Graham, Y. He and S. J. Berkowitz, 1992a, J. Appl. Phys., **71**, 4933 (1992).
10. T. D. Moustakas, T. Lei, R. J. Molnar, accepted for publication in Physica B.
11. T. D. Moustakas, R. J. Molnar, T. Lei, G. Menon and C. R. Eddy Jr., MRS Symp. Proc., **242**, 427 (1992).
12. T. Lei, PhD Dissertation, Boston University (1992)
13. C. Kittel, *Introduction to Solid State Physics*, 6th Ed., J. Wiley & Sons, New York, 1986.
14. M. Ilegems and H. C. Montgomery, J. Phys. Chem. Solids, **34**, 885 (1973).
15. I. Akasaki and H. Amano, MRS Symp. Proc. **242**, 383 (1991).
16. C. S. Hung and J. R. Gliessman, Phys. Rev., **96**, 1226.
17. N. F. Mott and T. D. Twose, Advances in Physics, **10**, 107 (1961).
18. T. L. Tansley and R. J. Egan, MRS Symp. Proc., **242**, 395 (1992)

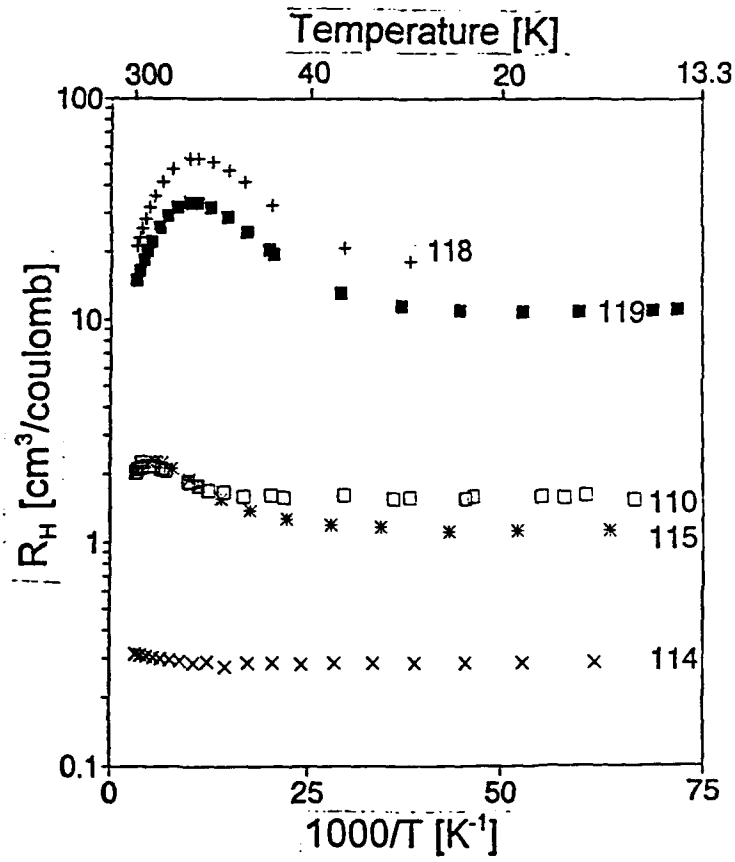

Figure 1 - Hall coefficient vs. 1/T.

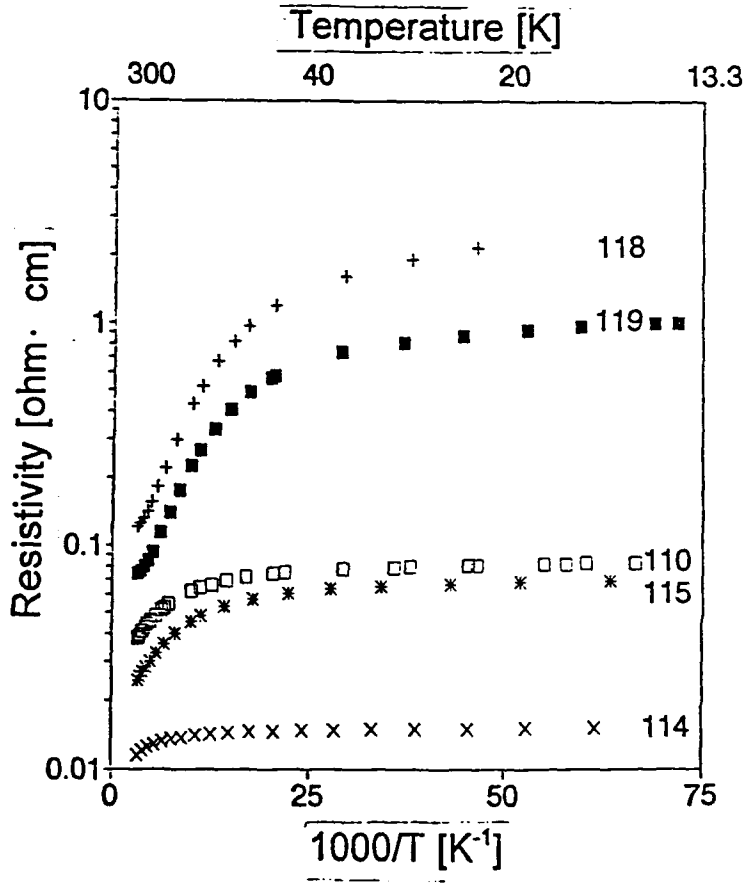

Figure 2 - Resistivity vs. 1/T.

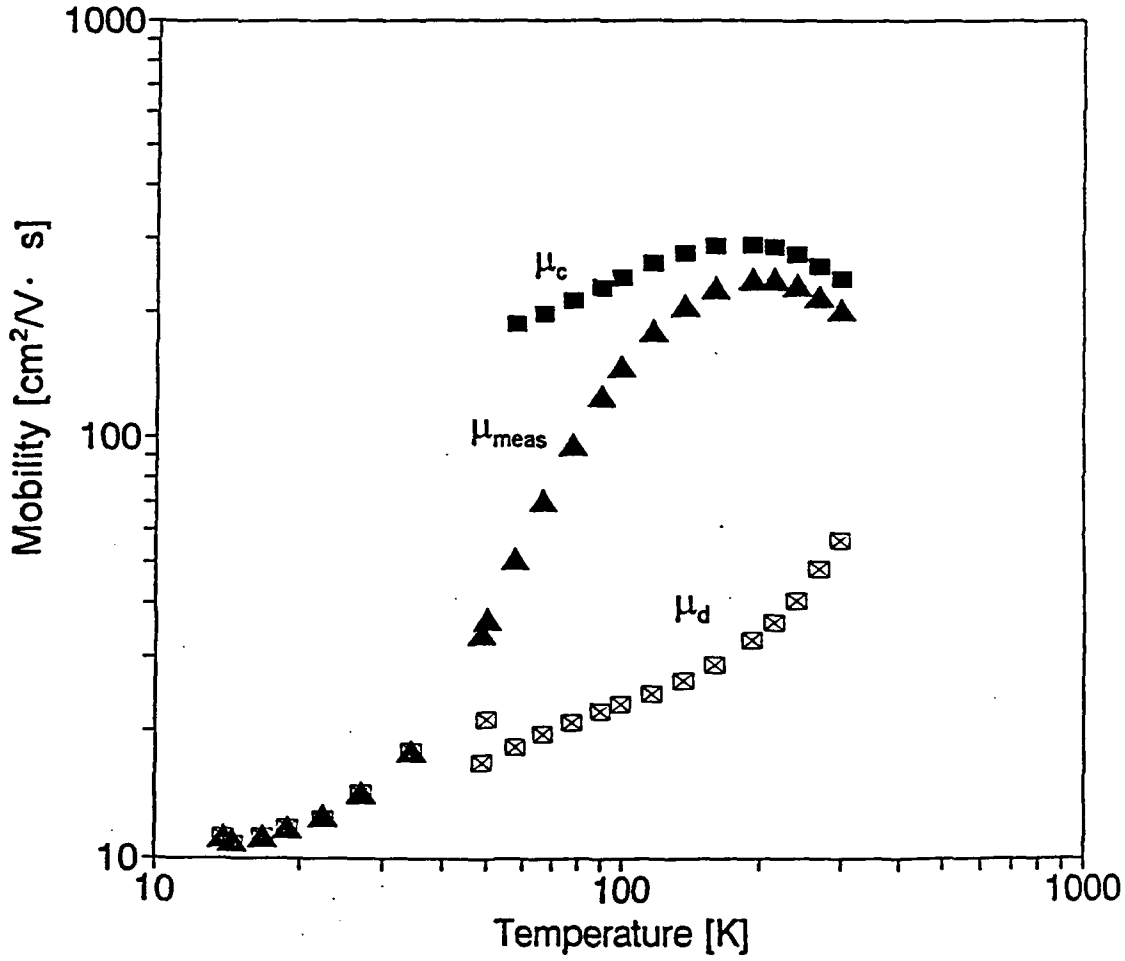

Figure 3 - Temperature dependence of μ_{meas}, μ_c and μ_d.

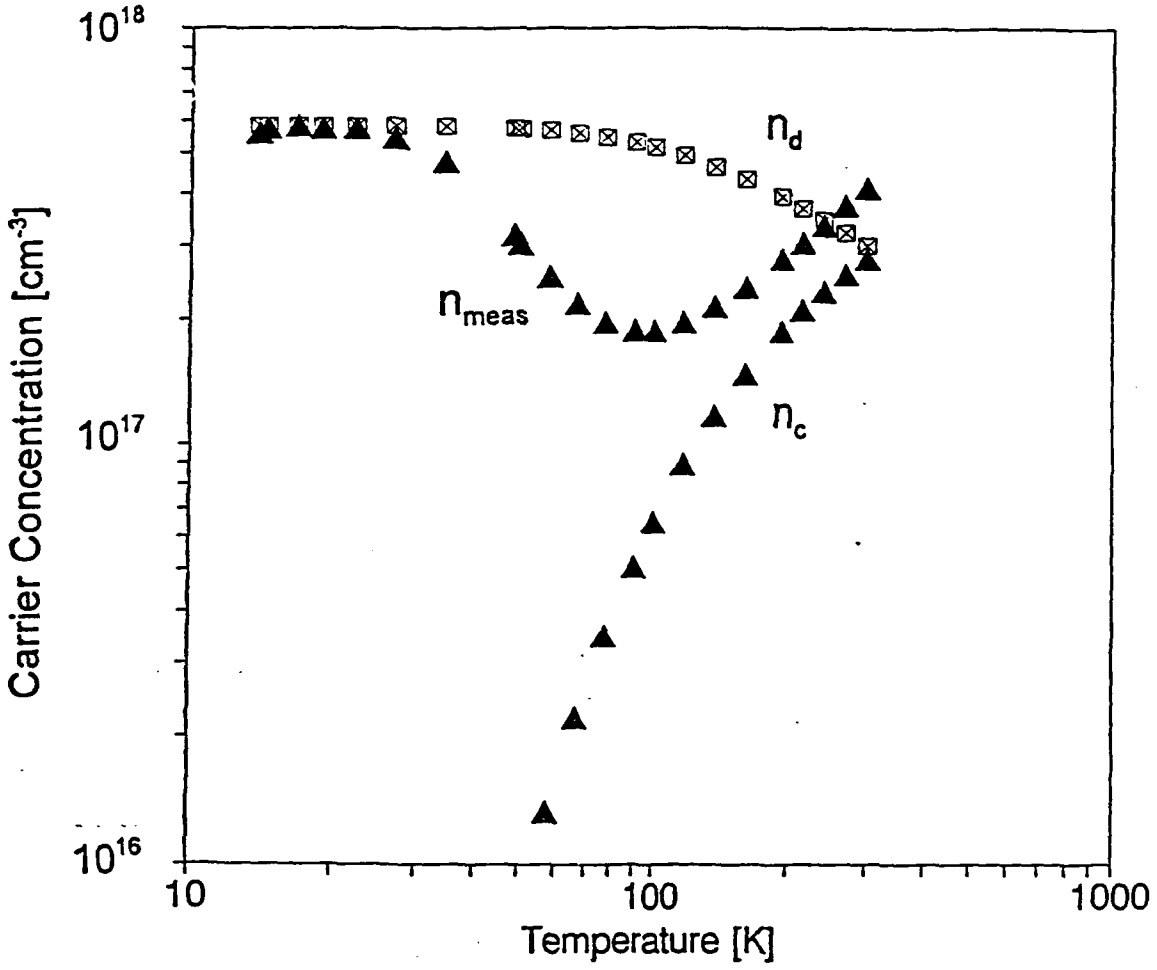

Figure 4 - Temperature dependence of n_{meas}, n_c and n_d.

Appendix D:

Metal Contacts to Gallium Nitride

submitted for publication
Applied Physics Letters

Metal Contacts to Gallium Nitride

J.S. Foresi and T.D. Moustakas

Boston University, Department of Electrical Engineering,
44 Cummington St., Bostor MA 02215.

Abstract

We report measurements on the nature of aluminum and gold contacts to GaN. The GaN films were deposited onto the R-plane of sapphire substrates by Molecular Beam Epitaxy and are autodoped n-type. Metal contacts were deposited by evaporation and were patterned photolithographically. Current-voltage characterization shows that the as-deposited aluminum contacts are ohmic while the as-deposited gold contacts are rectifying. The gold contacts become ohmic after annealing at 575°C, a result attributed to gold diffusion. The specific contact resistivity of the ohmic aluminum and gold contacts were found by transfer length measurements to be of device quality (10^{-7} - 10^{-8} Ωm^2). The results of these studies suggest a direct correlation between barrier height and work function of the metal, consistent with the strong ionic character of GaN.

Introduction

Gallium Nitride (GaN) is a direct, wide band-gap semiconductor ($E_g \simeq 3.4eV$) whose conduction band structure allows for a high saturation velocity (3×10^7 cm/sec) [1,2]. Due to these unique properties GaN is expected to find applilcations in optical devices (LED's, lasers, detectors) operating in the spectral region from the blue to near-UV and in electronic devices such as high temperature, high power, and high frequency transistors.

GaN films have been deposited heteroepitaxially on a variety of substrates by a number of vapor phase methods [3]. Such films are generally n-type with carrier concentrations between 10^{18} and 10^{20} cm^{-3} and electron moblities of about 20 $cm^2/V{\cdot}sec$. The n-type autodoping is attributed to nitrogen vacancies. The most important recent development is the discovery that AlN[4] and GaN[5-9] buffers lead to lateral growth which significantly improves the surface morphology and the electrical properties of the films. For example, films with carrier concentrations of 10^{16} and 10^{17} cm^{-3} and electron mobilities of 600 and 200 $cm^2/V{\cdot}sec$ were deposited by the Metalorganic Chemical Vapor Deposition (MOCVD) [4,9] and Electron Cyclotron Resonance assisted Molecular Beam Epitaxy (ECR-MBE) [8,10] methods respectively. Thus, the quality of GaN films is constantly improving and the succesful realization of devices and integrated circuits requires the development of standard semiconductor processing techniques. These include metal/GaN ohmic contacts and Schottky barriers, etching of GaN, formation of oxide or epitaxial barrier overlayers, diffusion of dopants and ion-implantation of active regions.

In this paper, we report our initial investigation of metal/GaN contacts. Metals investigated include Al and Au. Current-Voltage (I-V) measurements and transfer length measurements (TLM) of the specific contact resistivity are presented.

Experimental Method

The GaN films used in this study were grown by the ECR-MBE method without a GaN

buffer layer [11,12]. All films were deposited on sapphire substrates with R-plane orientation. X-ray diffraction studies show that the films have the wurtzitic crystal structure with $(11\bar{2}0)$ orientation, which leads to a faceted surface morphology[12]. The faceted surface makes these films unsuitable for planar devices. However, the metal contact results presented in this paper should be applicable to GaN films grown on other substrates and orientations. The transport coefficients were determined by Hall effect measurements using the Van der Paw configuration. The investigated films were n-type with resistivities of about $10^{-1}\Omega$·cm, carrier concentration of $3 \times 10^{18}\text{cm}^{-3}$ and Hall mobilities of about 20 $\text{cm}^2/\text{V}\cdot\text{sec}$. The thickness of the films were measured by scanning electron microscopy to be 1.6μm.

The Au and Al contacts were deposited on the GaN films by evaporation and patterned using photolithography and lift-off techniques [13]. The contacts were patterned in TLM structures which consist of three square contacts separated by known distances (see Figure 1a). The same contacts were also used in pairs to evaluate the rectifying nature of the metal/semiconductor interface by I-V characterization. Because these pairs of contacts were deposited on the surface of the GaN films, they constitued back-to-back Schottky barrier systems.

I-V characterization was carried out by injecting up to $\pm$20mA with a current source and measuring the voltage across the same contacts with an electrometer . I-V characterization was performed on both as-deposited metal contacts and on metal contacts which had been annealed in a reducing atmosphere for ten minutes at 575°C.

Measurements of the specific contact resistivity were made using the TLM method which is employed widely in the characterization of ohmic contacts to semiconductors[14-16]. The technique requires the formation of contacts with controlled geometry and evaluates the difference in resistance between equally sized pairs of contacts separated by different distances. The specific contact resistivity (ρ_c) is calculated from a measurement of the effective contact resistance (R_c), the contact width (W), and the transfer length (L_T):

$$\rho_c = R_c W L_T \tag{1}$$

The effective contact resistance is given by:

$$2R_c = \frac{R_2 l_1 - R_1 l_2}{l_1 - l_2} \tag{2}$$

where R_1 is the resistance measured between contacts spaced l_1 apart and R_2 is the resistance measured between contacts spaced l_2 apart. In a planar contact configuration, nearly all of the current enters the semiconductor through a small area at the edge of the contact [17]. The parameter L_T is the length of this area as indicated in Figure 1b. This quantity is estimated by plotting the resistance of two pairs of contacts against the distance separating the individual contacts within each pair. The line connecting the points R_1 and R_2 crosses the resistance axis at the $2R_c$ point and intersects the distance axis at the $-2L_T$ point (see Figure 1c).

The TLM technique relies on the assumption that the semiconductor material under the contact has not been doped differently than the bulk material, and the accuracy of the method depends on the ability to control the separation between the contacts. Due to the faceted surface morphology in our films, the determination of the contact areas was difficult

and limited the accuracy of the specific contact resistivity to within an order of magnitude.

Experimental Results and Discussion

The I-V characteristics of the as-deposited Al and Au contacts are shown in Figure 2. For both metals the I-V curves are symmetric about the origin as is expected for back-to-back Schottky barriers where the characteristic is that of a reverse-biased barrier irrespective of the current polarity [17]. The Al contact I-V characteristics are linear indicating that the contact is ohmic with no apparent barrier to current flow. In contrast, the I-V characteristics of the Au contact exhibit curvature associated with the formation of a Schottky barrier. This Schottky barrier is leaky due to tunnelling effects arising from the high carrier concentration of the films and the possible existance of an interfacial layer [13]. These results indicate that the barrier height depends on the metal used.

The I-V curves for the same contacts after annealing, shown in Figure 3, suggest that both the Al and Au contacts have changed during annealing. The I-V curves of the Al-contacts aquired a slight curvature and the calculated resistance increased by about 50%. These changes are consistent with the formation of an interfacial AlN-layer during the annealing process. The I-V curves of the Au-contacts became practically linear. A similar result has been observed in Au-contacts to GaAs and attributed to Au diffusion in GaAs [18].

The specific contact resistivities of Al and Au contacts were measured by the TLM method after annealing. The results are shown in Table I. All of the contacts measured have specific contact resistances in the 10^{-7} - $10^{-8}\Omega m^2$ range. The lowest specific contact resistivities reported for GaAs are $\simeq 10^{-9}\Omega m^2$ for high quality AuGeNi contacts [18]. The contact resistivities measured here are two orders of magnitude larger. However, their quality can be expected to be improved with better GaN material and more controlled processing and metallization.

The simplest considerations of Schottky barrier formation between metals and semiconductors rely on the difference in work functions of the two materials to predict the barrier height. For a large number of important semiconductors, Si and GaAs included, the dependence of barrier height on work function difference has not been observed, a result attributed to the existance of surface states which pin the Fermi level at the interface [19]. The dependence of the barrier height on the work function difference has been correlated to the ionicity of the semiconductor by Kurtin and co-workers [20] as shown in Figure 4. In this figure, the vertical axis is a parameter, S, which is defined as the change in barrier height over the change in metal work function. $(d\phi_b/d\chi_m)$ and the horizontal axis is the electronegativity difference between the components of a compound which is a measure of the compound's ionicity. The direct dependence of the barrier height on the work function for the semiconductors with large electronegativity differences results from the bunching of surface states near the band edges where they have less effect on the surface Fermi level position [17].

The electronegativity difference for GaN is 1.87eV[21,22]. This puts GaN above the knee of the curve implying that Schottky barriers on GaN should have barrier heights which depend directly on the work function difference between the metal and GaN. The work function of GaN has been measured to be 4.1ev[23]. Therefore, any metal with a work function equal to or lower than that of GaN should form essentially ohmic contacts to n-type GaN and any metal with a work function higher should form a rectifying contact to n-type GaN. The work fucntion of Al is 4.08ev[22] putting Al in the ohmic category. The

work function of Au is 4.82ev [22] which puts it in the rectifying category. Our results on Al and Au contacts to n-GaN are in agreement with the predictions of this model.

Based on these findings a variety of metals can be chosen to form either ohmic or Schottky barriers to n- or p-type GaN. For example, Al can form ohmic contacts to n-type GaN and Au can form ohmic contacts to p-type GaN. However, besides the work function, other factors may also play a role in choosing the proper metals for contacts to GaN. For example, Au appears to diffuse upon annealing in the GaN as has also been observed in GaAs. Thus, the use of Au as a contact to GaN requires a thin interlayer of Ti or Cr as a diffusion barrier [15]. Also annealing of Al contacts may result in the formation of a thin insulating AlN interlayer, which will increase its contact resistance.

Conclusions

In conclusion, the nature of Al and Au contacts to n-GaN were investigated. It was found that the as-deposited Al- and Au-contacts are ohmic and rectifying respectively. This result is in direct agreement with data indicating that ionic materials do not suffer from Fermi level pinning at metal/semiconductor interfaces. The lack of Fermi level pinning greatly reduces the complication of creating ohmic contacts to GaN as it is only necessary to determine metals with appropriate work functions. Al is appropriate for ohmic contacts to n-type and Au is appropriate for ohmic contacts to p-type materials. The implementation of Au contacts on GaN requires the use of a barrier metal to prohibit diffusion of Au into the GaN. Measurements of the specific contact resistivites of Al and Au annealed contacts on GaN give values in the range of $10^{-7} - 10^{-8}\Omega m^2$ which is of device quality.

Acknowledgement

The authors were benefited from collaborations with R. Molnar, W. Choi, and E. DeObaldia. Suggestions and discussions with Max Yoder and Scott Dunham are greatly appreciated. The work was supported partly by the Office of Naval Research (Grant Number # N00014-92-J-1436)

References

1. J.I. Pankove, MRS Symp. Proc. 162, 515 (1990)

2. P. Das, D.K. Ferry, Sol. State Electron., 19 (10), 1976

3. R.F. Davis, Proc. IEEE 79, 702 (1991)

4. I. Akasaki and H. Amano, MRS Symp. Proc. 242, 383 (1992)

5. G. Menon, M.S. Thesis (Boston University 1990)

6. T. Lei, M. Fanciuli, R.J. Molnar, T.D. Moustakas, R.J. Graham, and J. Scanlon Appl. Phys. Lett. 58, 944 (1991)

7. T. Lei, T.D. Moustakas, R.J. Graham, T. He and J. Berkowitz, J. Appl. Phys. 71, 4933 (1992)

8. T.D. Moustakas, T. Lei and R.J. Molnar, Physica B, Condensed Matter (1992)

Tabel I. Specific contact resistivities for Au/n-GaN and Al/n-GaN after annealing

Metal	Specific Contact Resistivity ($\Omega \cdot m^2$)	Metal	Specific Contact Resistivity ($\Omega \cdot m^2$)
Au	1.6×10^{-7}	Al	1.2×10^{-8}
	2.0×10^{-7}		4.4×10^{-7}
	3.1×10^{-7}		1.3×10^{-7}
	3.0×10^{-7}		

Figure Captions:

Fig.1 (a) Sample configuration for I-V and TLM characterization. The thin vertical stipe is a 10μm wide area of exposed GaN. The three wide rectangles are metal contacts separated by 20 and 15 microns. (b) Schematic of current flow through plannar contacts. Nearly all of the current flows through one transfer length, L_t, of the contacts' front edges. (c) Plot of the measured resistance against the contact separation.

Fig.2 I-V characteristics of as deposited Al/n-GaN and Au/n-GaN structures.

Fig.3 I-V characteristics of annealed Al/n-GaN and Au/n-GaN structures.

Fig.4 Dependence of $S = \frac{d\phi_b}{d\chi_m}$ (Change in barrier height over the change in metal work function) on the electronegativity difference between the components of the compound (After ref. 20)

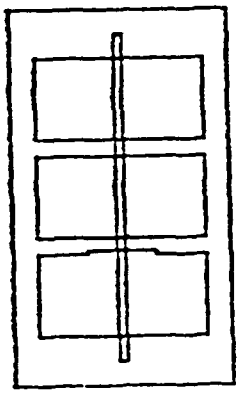

(a)

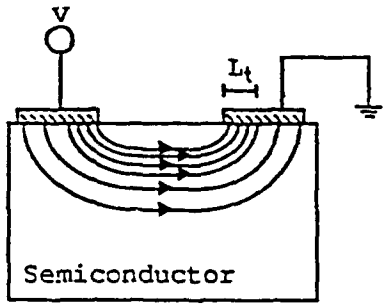

(b)

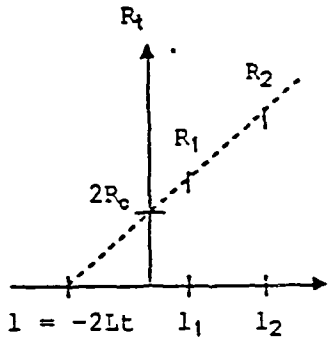

(c)

Fig. 1

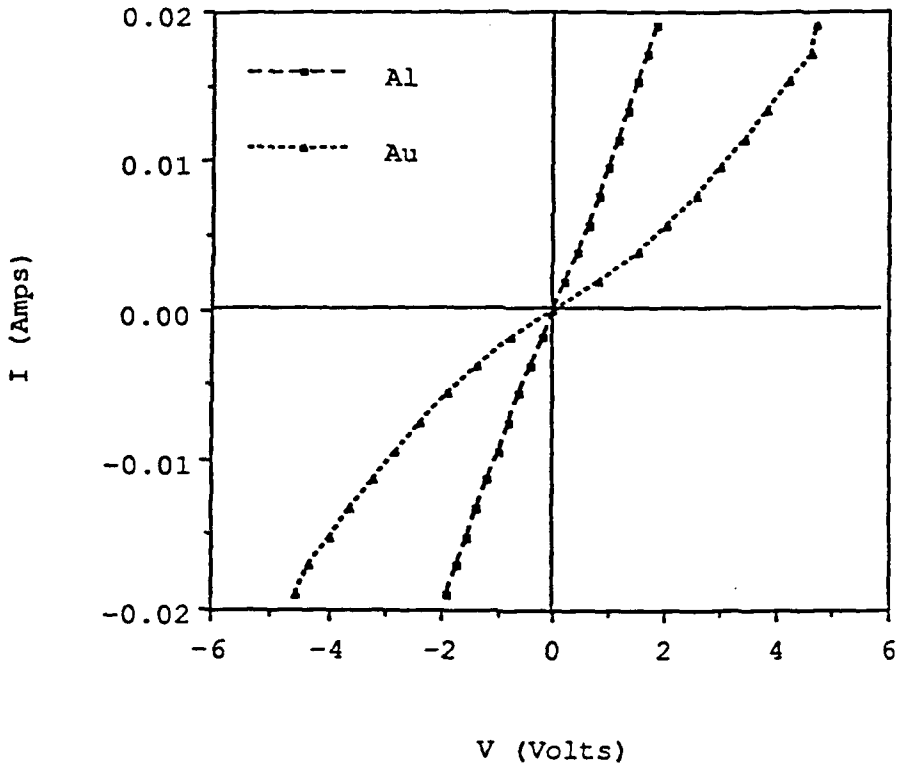

Fig. 2

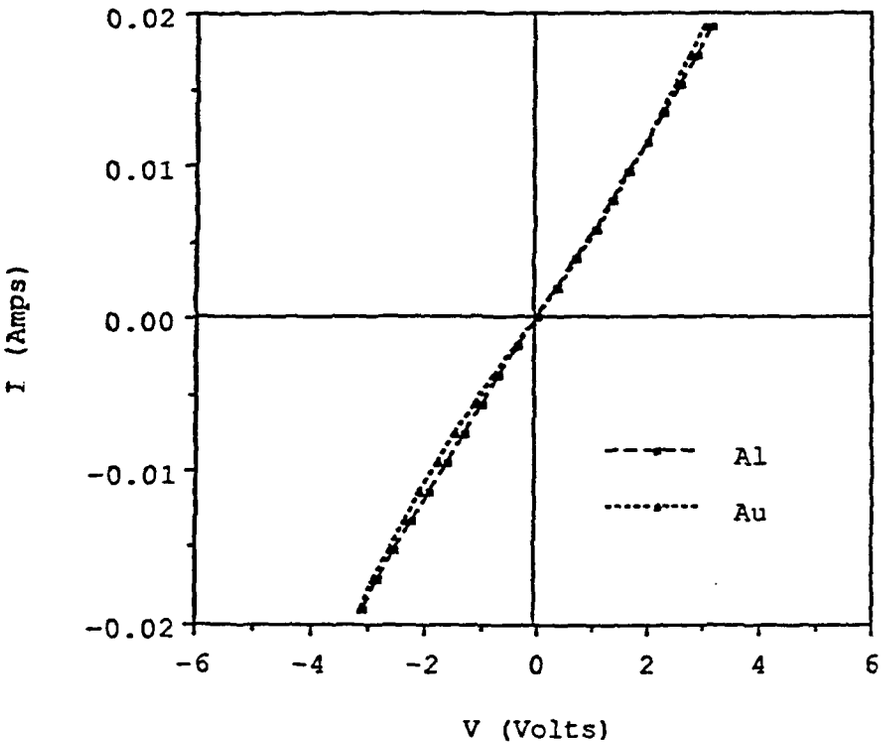

Fig. 3

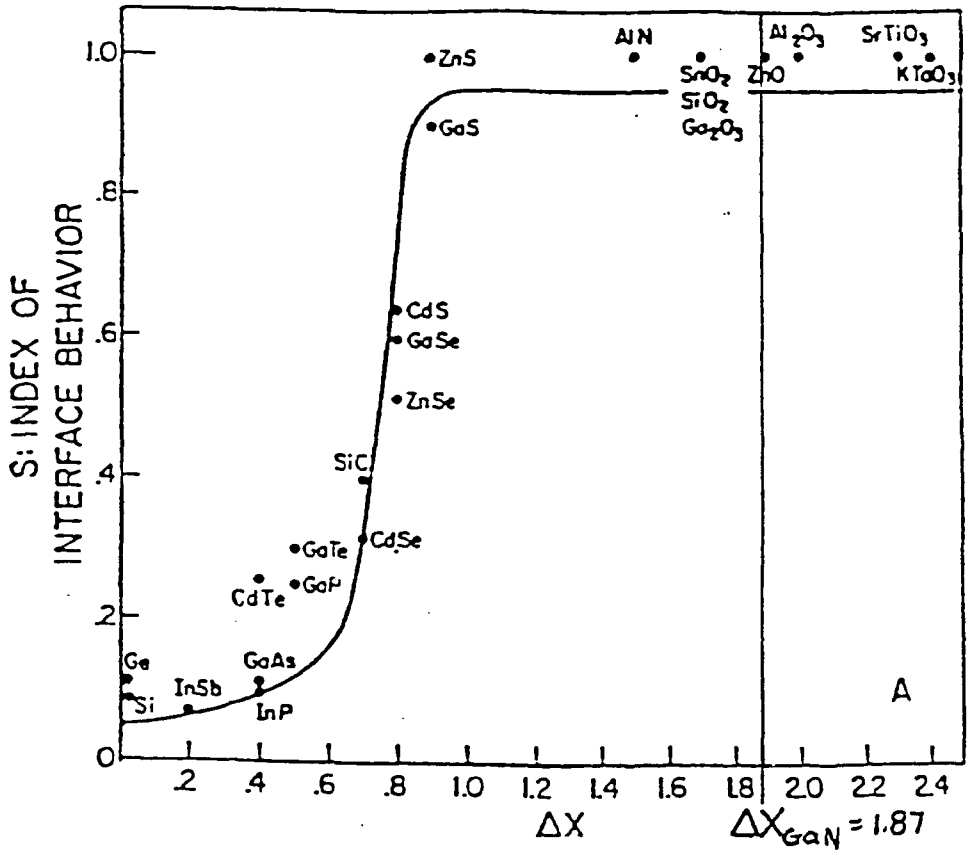
S: INDEX OF INTERFACE BEHAVIOR
1.0
.8
.6
.4
.2
0
ZnS
AlN
SnO_2
SiO_2
Ga_2O_3
Al_2O_3
ZnO
$SrTiO_3$
$KTaO_3$
GaS
CdS
GaSe
ZnSe
SiC
CdSe
GaTe
GaP
CdTe
Ge
Si
InSb
GaAs
InP
A
.2
.4
.6
.8
1.0
1.2
1.4
1.6
1.8
2.0
2.2
2.4
ΔX
$\Delta X_{GaN} = 1.87$

Fig. 4